Seismic Performance and Functional Recovery of Dual Lateral Load Resisting System Comprising of Coupled Structural Walls and Moment Resisting Frames

Sneha Benoy[1], Nicola Tondini[2], Saravanan M[3], & Vijayanarayanan AR[4*]

[1,4] Department of Civil Engineering, Amrita School of Engineering, Coimbatore, Amrita Vishwa Vidyapeetham 641112, India.

[2] Department of Civil, Environmental and Mechanical Engineering, University of Trento, Via Mesiano 77, 38123 Trento, Italy.

[3] CSIR-Structural Engineering Research Centre, Taramani, Chennai 600113, India.

Corresponding author: *ar_vijayanarayanan@cb.amrita.edu

ABSTRACT

The Coupling Ratio (CR) is one of the critical parameters for the design of coupled structural wall (CSW) systems. CR is defined as the proportion of lateral load resisted by the coupling beams relative to the total overturning moment resisted by CSW system. Previous studies recommend an optimal CR range of 30–70%, but these findings are largely based on isolated CSW systems. Consequently, the recommendation is not applicable for dual lateral load-resisting systems wherein the lateral loads are shared between moment resisting frames (MRFs) and CSW systems. For such dual lateral load-resisting systems, the CSW and MRFs are designed to resist the fraction of lateral load demand imposed on them. The demand, estimated during the analysis and design stage, depends on the initial elastic lateral stiffness of the system. However, during earthquakes, significant redistribution of lateral load may occur depending on the location and mode of damage to structural elements. This redistribution of forces may lead to undesirable performance during an earthquake. This underscores the need to establish optimal CR values for dual systems to ensure reliable seismic performance considering seismic performance at the building level. Again, with growing emphasis on post-earthquake functionality and resilience, it is equally important to understand how CR influences not only strength and ductility but also repairability, downtime, and economic loss. Thus, this study examines the effect of CR on the seismic performance of reinforced concrete CSW buildings designed as per Indian Standards. Three building configurations (10-, 12-, and 16-storey) are analyzed with CR values of 40%, 50%, and 60% using nonlinear static analyses. Performance metrics include fundamental period, base shear–drift capacity, inter-storey drift distribution, and ductility demand. Further, damage and loss assessments are undertaken across multiple peak ground acceleration (PGA) levels to quantify resilience. The results provide key insights into the role of coupling ratio in enhancing both seismic performance and resilience, offering practical guidance for the design of dual lateral load-resisting systems.

Keywords: Post-Earthquake; Resilience; Seismic Damage; Seismic Risk Assessment; Sustainable Urban Development.

1. Introduction

Coupled Structural Walls (CSW) system, which comprises of individual structural walls interconnected with coupling beams, are widely employed in buildings to resist lateral loads and control lateral displacement. Typically, slender structural walls with overall height to length ratio greater than 2 are considered for CSW system owing to its flexural behaviour during earthquakes [1,2]. The overall lateral load resistance of CSW system is governed by two primary actions, namely: (a) flexural action of the individual structural walls and (b) the frame action mobilised through the coupling beams. The latter induces axial forces demand in walls, the magnitude of which corresponds to the cumulative shear forces developed in the coupling beams (Fig 1. (a)). Furthermore, frame action of CSW system is primarily governed by the flexural and shear stiffness of the coupling beams. As a result, the overall behaviour of CSW system is strongly influenced by the stiffness characteristics of the coupling beams. This synergistic interaction between structural walls and coupling beams enhances the lateral stiffness of the CSW system, making it significantly greater than the combined stiffness of the individual walls acting independently as uncoupled elements [3]. Consequently, the seismic response of a CSW system is inherently distinct from that of a single uncoupled wall (Fig 1. (b)). In the case of the uncoupled wall, the lateral loads are resisted predominantly through the development of a base overturning moment ($M_{w,unc}$), as illustrated in Fig 1. (b).

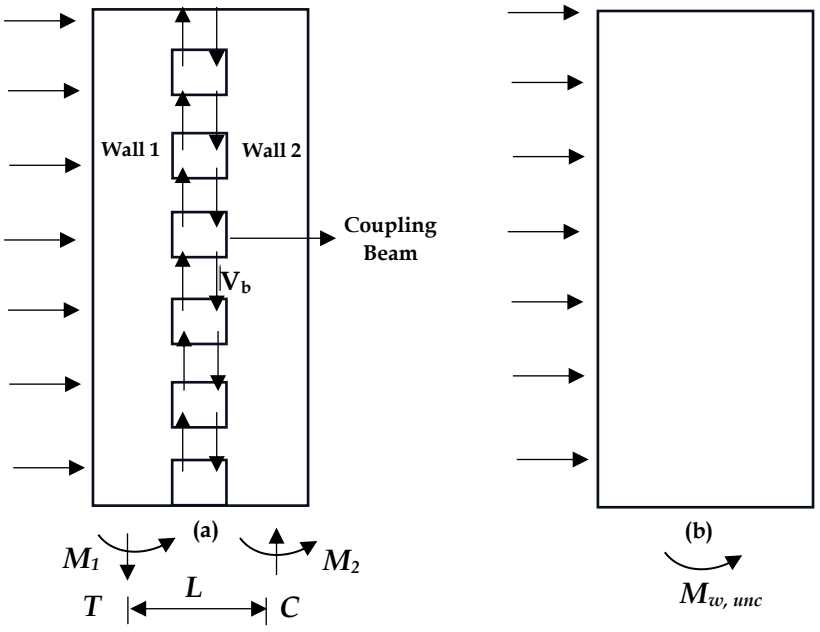

Fig 1. Wall systems (a) coupled wall (b) uncoupled walls

1.1 Seismic behaviour of CSW system

The seismic effectiveness of a CSW system is governed by the failure mechanism of its coupling beams. Coupling beams with a span-to-depth ratio less than or equal to two are prone to brittle shear failure. However, providing diagonal reinforcements in coupling beams (as recommended in codes) may lead to shear-flexural failure. Likewise, for coupling beams with span-to-depth ratio more than two, are controlled by either shear-flexural failure or flexural failure mode. In theory, the desired failure mechanism for a CSW system involves sequential formation of shear-flexural hinging in all coupling beams, followed by flexural hinging at wall base. This mechanism facilitates significant energy dissipation along the full building height [4,5]. The desired mechanism is akin to the *strong column-weak beam* design philosophy employed in ductile moment resisting frames.

To achieve the desired mechanism, CSW systems are proportioned and designed to attain a target Coupling Ratio (CR). The CR, also referred to as the degree of coupling, is defined as the fraction of the total overturning moment resisted by the coupling action (i.e., the frame action mobilised through the coupling beams as shown in Fig 1. (a). Quantitatively, CR is expressed as:

$$CR = \frac{TL}{M_1 + M_2 + TL} \tag{1}$$

where M_1 and M_2 is the moment of resistance at the base of structural walls 1 and 2, respectively; T is the axial force demand resulting from the coupling effect; and L is the center-to-center distance between structural walls (refer Fig 1. (a)).

The coupling ratio, a key parameter governing the interaction between structural walls and coupling beams in lateral force-resisting systems, has been shown to significantly affect the overall system stiffness, distribution of strength, sequence of yielding, and ductility characteristics of coupled structural wall (CSW) systems [6-10]. Recent experimental, and analytical, research on novel composite coupled wall systems [8,11] confirms that CR, design axial compression ratio, and structural aspect ratio strongly control yielding sequences of coupling beams and walls under cyclic seismic loads [12]. Recent literature recommends the use of higher CR values to ensure desired seismic performance through favourable yielding and full utilization of coupling actions [13]. Numerical studies indicate

88 that adopting higher CR value: (a) enhances the lateral load-resisting capacity of the CSW system and
89 (b) reduces the post-yield deformation capacity. Conversely, adopting lower CR values promote greater
90 system ductility [14]. Furthermore, literature indicate that adopting CR below 0.6 may result in poor
91 seismic behaviour as the coupling beams tend to yield prematurely relative to the wall piers, thereby
92 reducing the system's energy dissipation capacity and overall ductility [15]. Beyond the influence of
93 CR, the seismic performance of CSW system is influenced by other key parameters such as number of
94 stories, stiffness of boundary columns, and the length of coupling beams [15,16].

95 Therefore, selecting an appropriate CR is critical to achieving the desired seismic behaviour. In practice,
96 however, this selection often depends on designer's judgment and experience. In general, selecting a
97 low CR provides marginal structural benefit, as the corresponding reductions in wall moments and
98 lateral drifts are negligible. Conversely, selecting a higher CR impose large ductility demands on RC
99 coupling beams [6]. Additionally, CSW systems with low CR values (around 20%) are prone to higher
100 wall rotations and storey drifts, whereas those with higher CR values (around 60%) exhibit premature
101 crushing of walls and extensive cracking in the top portions of the wall [7]. Several studies recommend
102 CR between 20% and 60% to ensure efficient structural design [8-10]. Consistently, both the Egyptian
103 Code of Practice (ECP 203-2018) [17] and Eurocode 8 [18] prescribe a minimum CR of 25%. It is further
104 noted that the assumed effective flexural and shear stiffness of structural elements significantly affects
105 CR estimation and the associated design loads [19].

106 ***1.2 Seismic behaviour of dual frame system comprising of CSWs and MRFs***

107 For dual Lateral Load-Resisting Systems (LLRS) comprising structural walls and Moment Resisting
108 Frames (MRFs), the Indian Seismic code (IS 1893:2016) [20] recommends that the total base shear be
109 distributed between walls and frames in proportion to their relative lateral translational stiffness. In
110 addition, the code mandates the MRF alone be capable of resisting at least 25% of the total design base
111 shear. However, these provisions do not explicitly address dual LLRS comprising of CSWs and MRFs
112 (henceforth, termed as dual CSW–MRF system). Direct application of the same guidelines to such
113 systems may lead to undesirable design outcomes and seismic performance, primarily due to the
114 distinct role and expected damage of coupling beams during seismic loading.

115 During seismic action, damage to the coupling beams can: (a) reduce the coupling action of the CSW
116 system, and (b) significantly decrease the lateral stiffness of the CSW system. As the coupling action
117 deteriorates, the load-resisting mechanism in the CSWs transitions from axial-flexural interaction to
118 predominantly flexural behaviour in individual structural wall. Concurrently, the reduction in stiffness
119 causes a redistribution of lateral force demand, shifting a greater proportion of base shear to the
120 MRFs—potentially exceeding column's maximum shear capacity. Given the absence of specific design
121 guidelines that address the aforementioned effects, the overall seismic performance and resilience of
122 dual CSW–MRF system remains uncertain. This underscores the need to quantify the increased: (a)
123 lateral load demand in MRFs and (b) shear demands in columns part of MRFs, due to redistribution of
124 lateral force demand from CSW to MRF system during seismic action. Incorporating these
125 considerations into seismic design provisions would ensure that both CSW and MRF systems are
126 appropriately proportioned, designed and detailed to resist the expected demands. This is expected to
127 improve the robustness and seismic resilience of dual CSW–MRF system.

128 Furthermore, quantifying seismic damage is critical for evaluating the effectiveness of the seismic
129 design of structural systems [21,22]. At present, damage is typically assessed using global deformation
130 parameters such as roof drift and interstorey drift [23,24]. While these metrics provide a broad
131 indication of the overall structural damage, they fail to adequately capture the localized damage in
132 individual structural elements. In particular, member-level demands—such as plastic rotation demand
133 in beams and walls—requires more detailed assessment to accurately understand the structural
134 performance and failure mechanisms. Although several numerical studies [25-28] have investigated the
135 influence of CR in CSWs, there remains a lack of focused research assessing the seismic resilience of
136 dual CSW–MRF system. With growing emphasis on post-earthquake functionality and resilience [29-
137 31], it is equally important to understand the influences of CR on strength, ductility, repairability,
138 downtime, and economic loss of dual CSW–MRF system. Again, addressing this gap is essential to
139 develop a more comprehensive understanding of the overall seismic performance and failure
140 progression of such hybrid dual frame systems.

141 Building on the research gaps identified, this study aims to: (a) quantify the increased lateral force
142 demand in MRFs resulting from redistribution of seismic forces with progressive damage in the CSW

system, (b) recommend column design capacities required to preclude shear failure in structural members part of MRFs, and (c) evaluate the seismic performance of dual CSW–MRF system, including resilience assessment in terms of probable loss estimates and functional recovery. Phase 1 of the study addresses objectives (a) and (b), while Phase 2 focuses on objective (c).

To achieve the said objectives, the study presents preliminary numerical investigation into the seismic performance of RC dual CSW–MRF systems (proportioned with three distinct CRs – 40, 50 and 60%). Furthermore, three building configurations (with 10-, 12-, and 16-storeys) are considered to investigate the seismic performance of the said dual frame system. The details of study buildings are present in Section 2. The seismic performance of the system investigated using nonlinear static (pushover) analysis is presented in Section 3. The results of Phase 1 and 2 are present in Section 3.1 and 3.2, respectively. The scope of this study is limited to dual CSW–MRF systems, wherein the structural walls are proportioned and designed with rectangular cross-sections and are oriented along a single direction (i.e., X-direction). Although, soil-structure interaction influences the seismic response of the dual-frame system, the effects of the same are not considered in this study.

2. Numerical Analysis

The seismic performance of the study buildings is evaluated numerically using a commercially available software package [32]. The numerical investigation is conducted in two phases. In the first phase, the required shear capacity of columns part of MRFs is quantified. This assessment ensures that the dual CSW–MRF systems possess adequate lateral displacement capacity to withstand seismic actions. In the second phase, the seismic performance of a series of dual CSW-MRF system, designed in accordance with the recommendations derived from the first phase, is evaluated using nonlinear static (pushover) analysis. The present study considers a set of nine archetype reinforced concrete (RC) buildings designed as dual CSW–MRF system. The building set includes 10-, 12-, and 16-storey buildings, each with regular and symmetric plan geometry, as shown in Fig 2. (a). The plan layout features five bays in both the longitudinal and transverse directions, ensuring uniformity across all models. In each building, CSWs and MRFs are provided along the X-direction, while only MRFs are provided as the LLRS along the Y-direction. The coupled structural walls are located along the building

periphery to effectively enhance the stiffness and seismic resistance of the structure, in particular for torsional effects. The adopted layout of the CSW system is representative of commonly employed residential and office building typologies, as documented in relevant literatures [16,25,33,34].

Within each height category (say, 10-storey buildings), the CSW system is designed for three sets of coupling ratios (i.e., 40CR, 50CR and 60CR). This study considers three target coupling ratios—40%, 50%, and 60%—representing low, medium, and high coupling levels, respectively. The said range of CR is considered to quantify the influence of coupling ratio on seismic performance of dual CSW–MRF system. All buildings have identical plan layout, as illustrated in Fig 2. (a), while the elevation views corresponding to different storey heights are presented in Fig 2. (b).

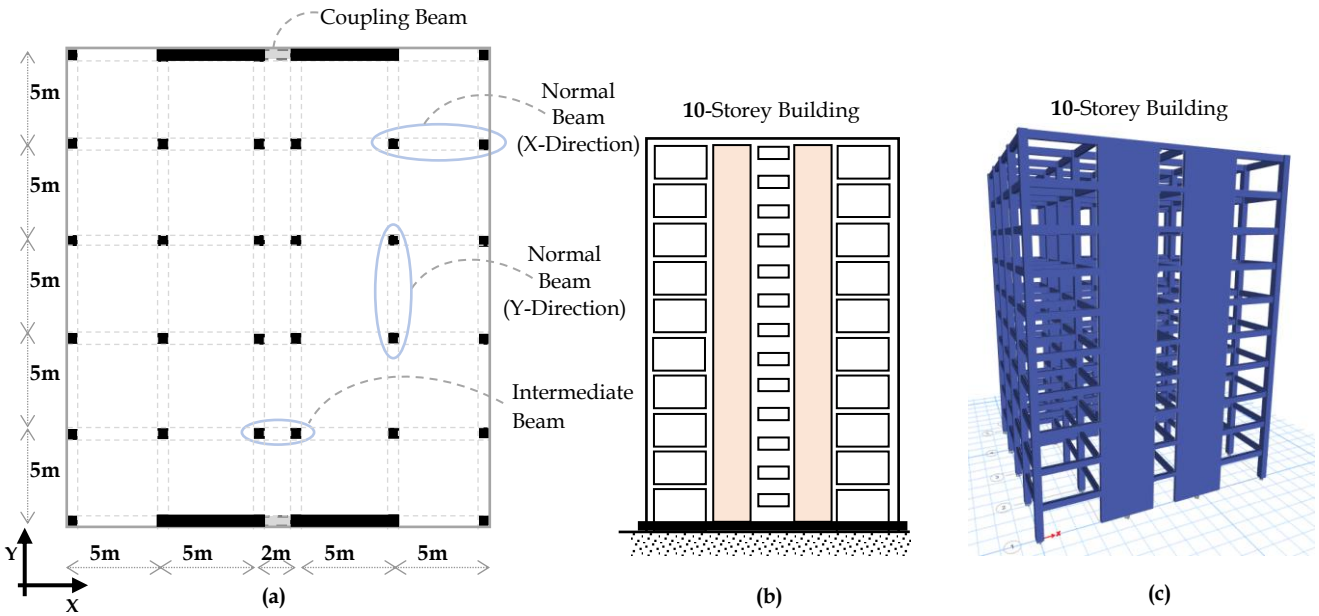

Fig 2. a) Floor plan view of the archetype buildings (b) Elevation of typical CSW building (c) 3D elevation

The length in X-direction is 22m and in Y-direction is 25m. The total height of 10-, 12- and 16-storey buildings were 30m, 36m, and 48m, respectively, with a uniform storey height of 3m. The coupling beams have a span of 2m. All buildings are considered with structural walls of length 5m (l_w) and thickness 0.3m (t_w). The slabs are assumed to be 150mm thick. The base of the ground storey columns is assumed to be fixed. The archetype buildings were designed using a concrete compressive strength of 30MPa and longitudinal reinforcement yield strength of 415MPa. Buildings are designed for gravity and seismic loads in accordance with IS 456:2000 [35], using appropriate load combinations. In addition, infill wall load representing 250mm thick wall is applied on the beams.

197 The basic live loads for typical floors and roof were considered as $3kN/m^2$ and $1.5kN/m^2$ respectively, as
198 per IS 875 (Part 2):1987 [36]. The beam-column joints are assumed to be rigid. The buildings are assumed
199 to be resting on hard soil stratum and situated at high seismic zone (Zone V) (with a peak ground
200 acceleration of $0.36g$), with an importance factor (I) =1 and response reduction factor (R) = 5. The
201 buildings are assumed to be located in Guwahati (Assam), in the Northeastern part of India. Lateral
202 force demands in each principal direction were obtained using response spectrum method by
203 combining the responses from at least three lateral translational modes, which led to a cumulative mass
204 participation exceeding 90% as recommended in literature [20].

205 In this study beams are categorized into three categories namely: (a) normal beams, (b) intermediate
206 beams, and (c) coupling beams (Fig 2. (a)). The normal beams have a span of $5m$ along X and Y-direction,
207 while both intermediate and coupling beams have a span of $2m$ along X-direction across all nine
208 buildings. Beams and columns are modelled as line elements and slab is modelled as a rigid diaphragm.
209 Columns are assumed to be axially rigid while remaining flexible in the lateral directions. Coupled
210 structural walls are modelled using the two-dimensional equivalent frame method (Fig 3.), which has
211 been widely adopted in previous studies to investigate the nonlinear seismic response of CSWs [37-40].
212 Individual structural wall is modelled using wide-column analogy wherein the wall is idealized as a
213 column element located at the centroid of the wall section. Rigid line elements are used to connect the
214 coupling beams to the centerlines of the walls. Effective moment of inertia of beams and columns are
215 assumed to be less than that of the gross moment of inertia. Stiffness modifiers for beam, column and
216 structural wall elements (*i.e.*, I_{eff} of beams = 0.4 I_{gross} and I_{eff} of columns and structural walls = 0.7 I_{gross})
217 were adopted according to the recommendations available in the literature [20] to account for cracked
218 section properties. For coupling beams, the effective moment of inertia is computed based on the
219 recommendations available in literature [41]; the same is reproduced below for reference:

220
$$I_{eff} = \frac{0.4 I_{gross}}{\left[1 + 3\left(\frac{h}{l_c}\right)^2\right]} \tag{2}$$

221 where, h is the depth of the beam and l_c is span of the coupling beam

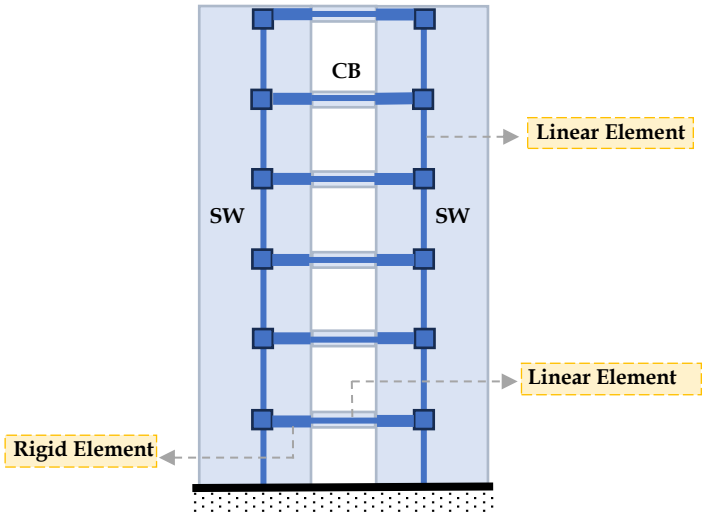

Fig 3. Equivalent frame model for coupled wall system

The CR of the 2D-CSW system was estimated using Eqn. (1), considering code-recommended [20] distribution of lateral load along the building height. In practice, achieving a target CR is an iterative process that requires proportioning the geometric properties of both coupling beams and structural walls. The iterative procedure adopted in this study is illustrated in Fig 4. After proportioning the structural elements (i.e., coupling beams and structural walls) to attain the target CR, the 3D dual CSW–MRF system was modelled. Subsequently, a linear elastic analysis of all nine-3D dual CSW–MRF system was undertaken to determine the design base shear and corresponding equivalent lateral force distribution, in accordance with IS 1893:2016 [20]. Modal analysis was conducted to determine the natural periods and mode shapes of the 3D dual CSW–MRF system (Fig 2. (c)). Subsequently, response spectrum analysis was performed to estimate the seismic lateral load demands. Finally, the adequacy of the initially assumed member proportions was then re-examined considering the updated lateral load estimates obtained from the response spectrum analysis.

To facilitate a direct comparison among study buildings, the beam and column sizes in the moment-resisting frames were maintained identical across all buildings (with the exception of 16-storey buildings where the column sizes were increased by 16% - refer Table 1). Variations were introduced only in the geometry of the coupling beams, which were tailored to attain target CRs. The geometric properties of structural elements adopted in the study is summarised in Table 1. For clarity, each building is denoted based on the number of storeys and coupling ratio. For instance, C10_40 represents a 10-storey building with a 40% coupling ratio.

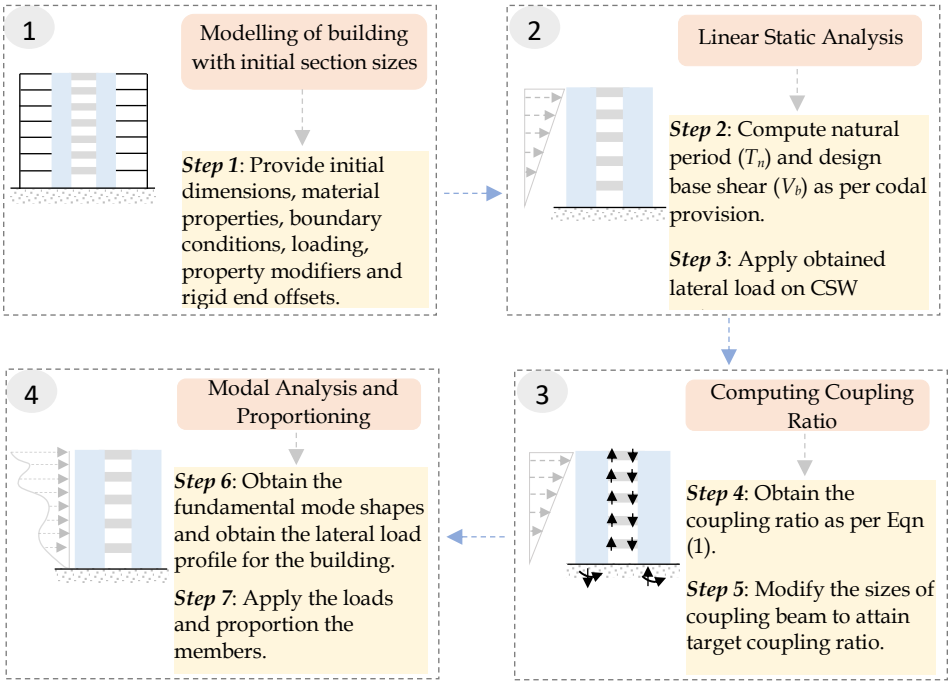

Fig 4. Flowchart for initial proportioning of buildings

The study buildings were designed and detailed in accordance with IS 456:2000 and IS 13920:2016 [2,35]. All structural elements were proportioned following capacity design principles to (a) promote flexural hinging while preventing shear failure, and (b) concentrate inelastic action in beams rather than columns. Coupling beams were designed for maximum shear capacity to enhance overall displacement ductility. Furthermore, none of the coupling beams met the criteria for the provision of the diagonal reinforcement in coupling beams as stated in IS 13920:2016 [2]. Accordingly, all coupling beams were detailed with conventional longitudinal reinforcement supplemented by closely spaced transverse stirrups to resist the imposed shear demands.

A summary of reinforcement detailing for the nine building models is presented in Annex A, Table A1. The longitudinal and transverse reinforcement ratios in beams was maintained within the following ranges: 10-storey buildings: 0.33%–1.47% (longitudinal), 0.07%–0.11% (transverse); 12-storey buildings: 0.33%–1.74% (longitudinal), 0.07%–0.12% (transverse); and 16-storey buildings: 0.33%–2.12% (longitudinal), 0.11% (transverse). For columns, the longitudinal reinforcement ratio ranged between 0.85% and 4.19%, while transverse reinforcement ratio ranged between 0.03% and 0.09% for all buildings. Structural walls were provided with longitudinal reinforcement ratio in the range of 2.44%–3.01%, and transverse reinforcement of approximately 0.05%.

Table 1. Geometric properties of structural elements in study buildings

Building		C10_40	C10_50	C10_60	C12_40	C12_50	C12_60	C16_40	C16_50	C16_60
Beams Depth (*in mm*) Width: 300mm	Normal	550	550	550	500	500	500	550	550	550
	Intermediate	300	300	300	300	300	300	300	300	300
	Coupling	410	540	710	360	470	650	300	380	510
Square Column (*mm*)		600	600	600	600	600	600	700	700	700
Structural Wall (*mm*)		5000 x 300								
Seismic Weight (*kN*)		61,571	61,610	61,661	74,125	74,164	74,229	1,03,634	1,03,672	1,03,734
Design Base Shear, V_B (*kN*)	*X-Direction*	2,695	2,697	2,699	2,777	2,778	2,781	3,068	3,069	3,071
	Y-Direction	3,671	3,674	3,677	3,683	3,685	3,688	3,862	3,864	3,866

Material nonlinearity was represented using a lumped plasticity approach for beams, with concentrated plastic hinges assigned at both ends of each member [42]. Flexural hinges were modeled using the Modified Ibarra–Medina–Krawinkler (IMK) deterioration model [43], with a trilinear backbone to account for the cyclic strength and stiffness degradation, thereby simulating post-yield seismic behavior. For RC structural walls and columns, a fibre-based nonlinear modeling approach was adopted [44]. In this method, each cross-section was discretized into multiple fibres. Confinement effects in concrete were incorporated using Mander's model recommended in the literature [45]. Each column cross-section was discretized into 16 fibres for confined and unconfined concrete, along with 12 fibres for longitudinal reinforcement (Fig 5). Shear failure in moment-resisting frame components was precluded through capacity design. Nonetheless, force-controlled shear spring were assigned to beams, columns, and structural walls to monitor shear demand and safeguard against brittle failure. Location of flexural hinges and potential shear springs in structural elements were adopted as per ASCE 41-17 [46], and is summarized in Table 2. The fibre hinge locations for columns and structural walls are based on the expected locations of maximum demand considering the applied loads. Fig 5. provides an overview of the modeling assumptions and schematic diagram of idealized backbone curves. All study buildings were evaluated using nonlinear static (pushover) analysis (NSA) to assess seismic performance. Lateral loads, derived from response spectrum analysis, were incrementally applied until the buildings reached their failure mechanism. P-delta effects were included to capture the geometric nonlinearity. The NSA was terminated when either the displacement capacity of the

flexural hinge or the ultimate shear capacity of the structural elements reached its ultimate limiting value.

Table 2. Type and location of hinges assigned to structural elements

Element	Type of Hinge	Location of Hinge
Beams	Lumped plastic hinge	At a distance of half the beam depth from the column face
	Shear spring	At a distance of beam depth from the column face
Columns	Fiber hinge	At a distance of half the column depth from the beam face
	Shear spring	At a distance of column depth from the beam face
Structural Wall	Fiber hinge	At the base of the structural wall
	Shear spring	At a distance of half the structural wall length from its base

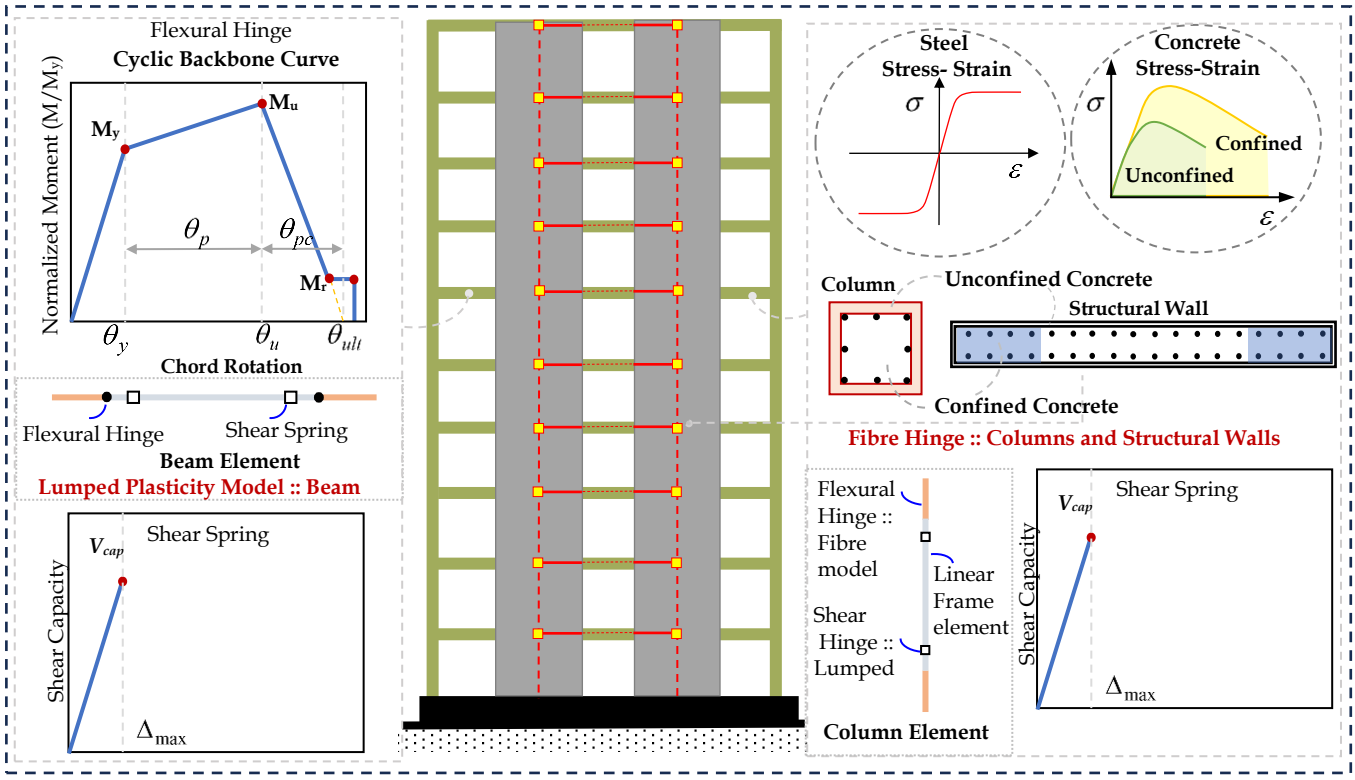

Fig 5. Graphical representation of the nonlinear modelling considered in this study

3. Results and Discussions

3.1 Phase 1: Influence of columns shear capacity on seismic behaviour of Dual CSW–MRF system

For all study buildings, the columns (part of MRF) were initially designed in accordance with IS 13920:2016. However, results from the NSA revealed that the lateral displacement capacity of the dual CSW–MRF systems was governed by shear failure of the MRF columns. As shear failure is inherently brittle, it is regarded as an undesirable failure mode. Such a failure was observed due to significant

yielding of coupling beams, which in turn reduced the lateral translational stiffness of CSW system leading to significant redistribution of base-shear between the CSW and MRF systems. For brevity, the detailed discussion on the base shear distribution between the CSW and MRF systems is omitted here but is provided in Section 3.2.(e).

To address the reduced displacement capacity of dual CSW-MRF system, the shear capacities of the MRF columns were increased (and expressed as a proportion of their maximum nominal shear capacity). As per design, the columns maximum shear capacity across all buildings ranged between 16% to 49% of the maximum nominal shear capacity. Here, the maximum nominal shear capacity (= $\gamma_m \times \tau_{c\max} \times bd$) for a given concrete grade was determined as the product of the partial safety factor for concrete in shear (1.18, as specified in SP 16:1978 [47]), the maximum shear stress associated with diagonal compression failure of concrete, and the column cross-sectional area. Fig 6. (a) presents the normalized lateral force-displacement response of a representative CSW-MRF system (16S_40CR) with MRF columns designed considering (a) increased shear capacity (=50% of maximum nominal shear capacity = $0.5 \times \gamma_m \times \tau_{c\max} \times bd$) (denoted as 16S_40CR_C1) and (b) the shear capacity recommended by IS 13920:2016 (denoted as 16S_40CR_C2).

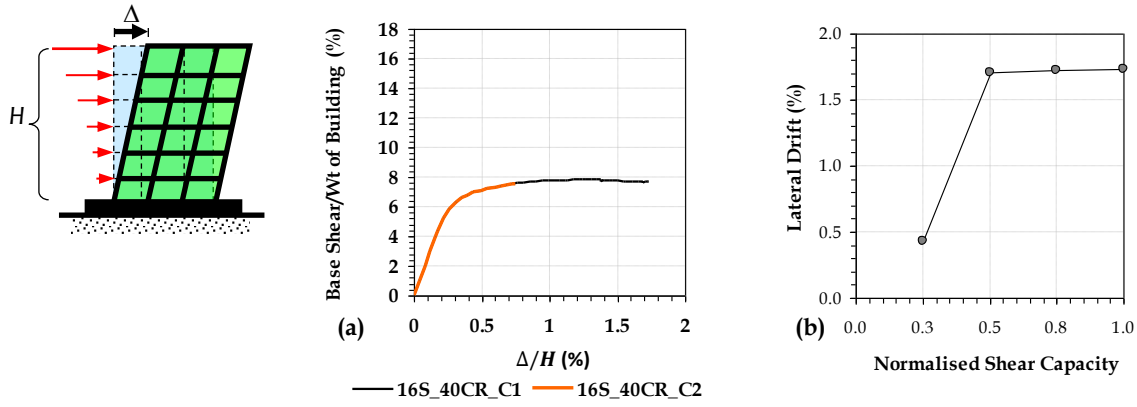

Fig 6. (a) Normalised base shear versus drift (=Roof displacement (Δ)/total height (H)) for a dual CSW–MRF systems (16S_40CR) with distinct column shear capacities (b) variation in the lateral drift capacity of dual CSW–MRF systems with gradual increase in the column shear capacity (Normalised shear capacity = provided shear capacity/maximum shear capacity).

The dual CSW–MRF system with increased nominal column shear capacity exhibited a lateral displacement capacity approximately 2.27 times greater than that designed with the IS 13920:2016-based shear capacity. This improvement is attributed to the prevention of brittle shear failure in the

MRF columns. It is noteworthy, however, that increasing the shear capacity beyond 50% of the maximum nominal shear capacity did not result in substantial enhancement of lateral displacement capacity (Fig 6. (b)). This finding suggests that MRF columns should be designed with shear capacities exceeding 50% of their maximum nominal shear capacity to ensure desired seismic performance.

3.2 Phase 2: Seismic Behaviour of Dual CSW–MRF system

For all nine buildings, the shear capacity of the MRF columns was set to 50% of the maximum shear capacity of the column section. This assumption was adopted to (a) ensure that the dual CSW–MRF system attains its maximum lateral displacement capacity, and (b) preclude shear failure in the MRF columns.

(a) Modal Characteristics of Dual CSW–MRF system

Table 3 lists the fundamental periods and modal properties of study buildings along X-direction. In general, it is observed that the natural period increased with building height, being largest for the 16-storey buildings and lowest for the 10-storey buildings. Increasing the coupling ratio from 40CR to 60CR reduced the fundamental period by about 20% in 10-storey, 19% in 12-storey, and 13% in 16-storey buildings, reflecting higher lateral translational stiffness for CSW–MRF system with higher CR. In all cases, the first mode dominated the seismic response, contributing 70–73% of mass participation, while the second and third modes accounted for 13–16% and 5–6%, respectively. The effect of CR on modal properties was more significant in shorter buildings, whereas taller buildings exhibited reduced sensitivity due to increased wall flexibility.

Table 3. Fundamental natural period and modal properties in X-direction

Buildings	T_1(s)	T_2(s)	T_3(s)	Mass Participation Factor		
				M_1	M_2	M_3
C10_40	0.813	0.202	0.088	71%	16%	6%
C10_50	0.747	0.192	0.086	72%	15%	6%
C10_60	0.655	0.173	0.08	73%	15%	6%
C12_40	1.152	0.287	0.124	70%	15%	6%
C12_50	1.059	0.273	0.121	71%	15%	6%
C12_60	0.935	0.248	0.113	72%	14%	6%

C16_40	1.605	0.428	0.192	72%	13%	5%
C16_50	1.52	0.413	0.189	72%	13%	5%
C16_60	1.394	0.386	0.181	72%	13%	5%

384

385 ***(b) Base Shear vs. Lateral Drift Response of Dual CSW–MRF system***

386 Fig. 7 illustrates the base shear versus lateral (roof) drift response from the pushover analysis of the
387 study buildings along X-direction. Key seismic characteristics of the study buildings are listed in Table
388 4. For buildings with same height, both yield strength (F_y) and ultimate strength (F_u) exhibits a gradual
389 increase with higher CR. This trend indicates that the lateral strength capacity of the building, in both
390 elastic and inelastic ranges, enhances due to the provision of stiffer coupling beams (i.e., higher CR).
391 Similarly, the lateral translational stiffness (K) also increases by approximately 22–52% as the coupling
392 ratio increases from 40 to 60%. Again, the increase in K can be directly attributed to the overall increase
393 in the lateral translational stiffness of CSW system due to the provision of stiffer coupling beams.
394 Additionally, the overstrength ratio (Ω=F_u/design lateral force) follows a comparable trend improving
395 about 6 to 15% with higher CR values. Conversely, the ultimate displacement capacity (Δ_u) indicates a
396 decreasing trend – reducing by approximately 6 to 38% – with increase in CR (from 40 to 60). This
397 reduction can be attributed to the provision of stiffer coupling beams, which may lead to structural
398 elements reaching their flexure/shear ultimate capacity relatively sooner. Except for 10-storey
399 buildings, the yield displacement (Δ_y) also decreases by 26–32% with an increase in CR, likely for similar
400 reasons, as stiffer coupling beams tend to promote earlier yielding of the primary lateral load–resisting
401 elements. In summary, buildings with higher CR exhibited higher lateral translational stiffness, higher
402 lateral strength and lower lateral displacement capacity. Conversely, buildings with lower CR exhibited
403 lower translational stiffness, lower lateral strength and higher lateral displacement capacity. Lastly, as
404 expected, for buildings with same CR, the lateral translational stiffness decreases with increase in
405 building height. Conversely, for buildings with same CR, the yield displacement (and ultimate
406 displacement) increases with increase in building height. The observed trends are similar to trends
407 reported in the literature [48].

408

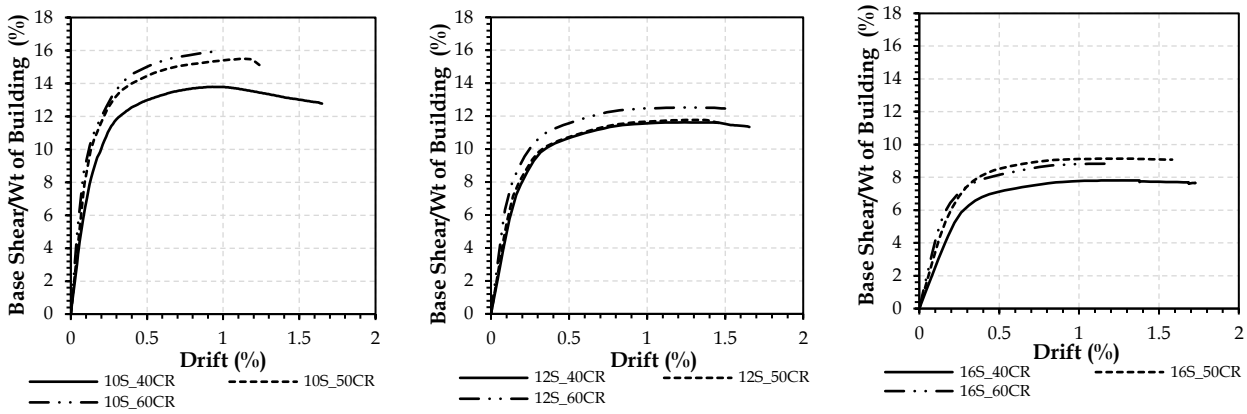

Fig 7. Normalized base shear versus lateral roof drift for dual CSW–MRF system with different CRs (a) 10-storey (b) 12-storey and (c) 16-storey building (seismic weight is available in Table 1)

Table 4. Key characteristics from lateral force-displacement response of dual CSW–MRF system

Building	***10-Storey***			***12-Storey***			***16-Storey***		
Coupling Ratio (%)	*40 CR*	*50 CR*	*60 CR*	*40 CR*	*50 CR*	*60 CR*	*40 CR*	*50 CR*	*60 CR*
Yield Strength, F_y (*kN*)	4337	6096	6315	5814	5925	5778	6066	6375	6686
Ultimate Strength, F_u(*kN*)	8492	9542	9803	8618	8728	9284	8098	9466	9153
Translational Stiffness, K (*kN/mm*)	140	160	171	86	91	126	48	65	73
Yield Displacement, Δ_y (*mm*)	31	38	37	68	65	46	126	98	92
Yield Drift (%)	0.10	0.13	0.12	0.19	0.18	0.13	0.26	0.20	0.19
Ultimate Displacement, Δ_u (*mm*)	495	375	309	596	525	556	829	759	562
Ultimate Drift (%)	1.65	1.25	1.03	1.66	1.46	1.54	1.73	1.58	1.17
Over Strength (=*ultimate strength/design lateral force*)	3.2	3.5	3.6	3.1	3.1	3.3	2.6	3.1	3.0

(c) Performance Point and Displacement Ductility of Dual CSW-MRF system

Table 5 presents the seismic performance points obtained using nonlinear static analysis of all study buildings, expressed in terms of lateral drift demand, for ten design acceleration levels. These performance points were evaluated following the stepwise procedure outlined in the literature [49]. In general, the performance point represents the equilibrium state between the structure's capacity and the seismic demand, and is obtained by superimposing the capacity curve and the demand spectrum. Prior to this superimposition, the curves are modified to account for hysteretic and viscous energy dissipation effects, ensuring a realistic representation of inelastic demand on buildings for different shaking intensities. It is observed that the lateral drift demand increases with the intensity of ground shaking. However, for buildings of the same height subjected to identical seismic excitation, the lateral drift demand tends to decrease with increasing coupling ratio (CR). For example, in the 10-storey

building under a PGA of 0.75*g*, the lateral drift demand for the 40 CR configuration is 0.39%, while that for the 60 CR configuration reduces to 0.31%—approximately 26% lower. This reduction can be attributed to the enhanced lateral translational stiffness provided by the stiffer coupling beams in buildings with higher CR values. Thus, buildings designed with higher CR exhibit relatively lower lateral drift capacities and drift demands compared to those designed with lower CR values (Table 4 & Table 5). To maintain consistency, the discussions presented in the subsequent sections (i.e., Sections 3.2 (e) to (i)) describe the seismic performance of the buildings corresponding to the lateral displacement demands at different PGA levels.

Table 5. Lateral displacement demand corresponding to performance points for dual CSW–MRF system for different PGA levels

Building Details	**PGA (*g*) (corresponding to design basis earthquake)**									
	0.16	0.24	0.36	0.45	0.55	0.65	0.75	0.85	0.95	1
	Lateral Drift (%) corresponding to performance points									
10S_40CR	0.07	0.11	0.16	0.20	0.27	0.33	0.39	0.45	0.50	0.50
10S_50CR	0.08	0.10	0.14	0.17	0.22	0.28	0.35	0.41	0.47	0.48
10S_60CR	0.06	0.09	0.13	0.17	0.23	0.29	0.31	0.34	0.39	0.41
12S_40CR	0.06	0.12	0.18	0.22	0.27	0.33	0.39	0.46	0.53	0.58
12S_50CR	0.06	0.11	0.16	0.20	0.26	0.32	0.38	0.45	0.52	0.56
12S_60CR	0.08	0.10	0.14	0.18	0.23	0.30	0.37	0.41	0.44	0.46
16S_40CR	0.10	0.14	0.21	0.26	0.31	0.36	0.42	0.48	0.55	0.59
16S_50CR	0.09	0.13	0.18	0.22	0.27	0.32	0.38	0.44	0.50	0.54
16S_60CR	0.08	0.11	0.16	0.20	0.24	0.29	0.34	0.41	0.48	0.53

(d) Redistribution of demand within coupled structural wall system (i.e., walls and coupling beam)

As discussed in Section 3.1, damage to coupling beams with increasing displacement demand leads to a progressive reduction in their rotational restraint on the adjoining structural walls. Consequently, the coupling interaction between the walls diminishes, reducing the overall CR. Fig 8. illustrates this reduction in CR with increasing lateral displacement under nonlinear static analysis. As the coupling action weakens, the proportion of overturning moment resisted by the coupling beams decreases, while the corresponding demand on the structural walls increases. This redistribution results in higher strength and deformation demands on the walls. For all buildings, the CR values estimated from NSA, particularly at low interstorey drift levels, deviate from those assumed during the design stage. This discrepancy arises from differences in the lateral load profiles and system configurations used to compute CR at each stage. Specifically, during design, CR is evaluated by applying an inverted

triangular lateral load distribution on the CSW system alone (i.e., coupling beams and structural walls). In contrast, during NSA, CR is determined under the design lateral force distribution applied to the dual CSW–MRF system, which includes both the CSW and MRF components. Despite these methodological differences, the extent of CR reduction with increasing drift is observed to be smaller in the 16-storey building compared to the 10-storey model. For example, at 0.4% lateral drift, the CR for the 10S_60CR building reduces to 38%, whereas the corresponding value for the 16S_60CR building remains higher at 46%, indicating improved coupling stability in taller systems.

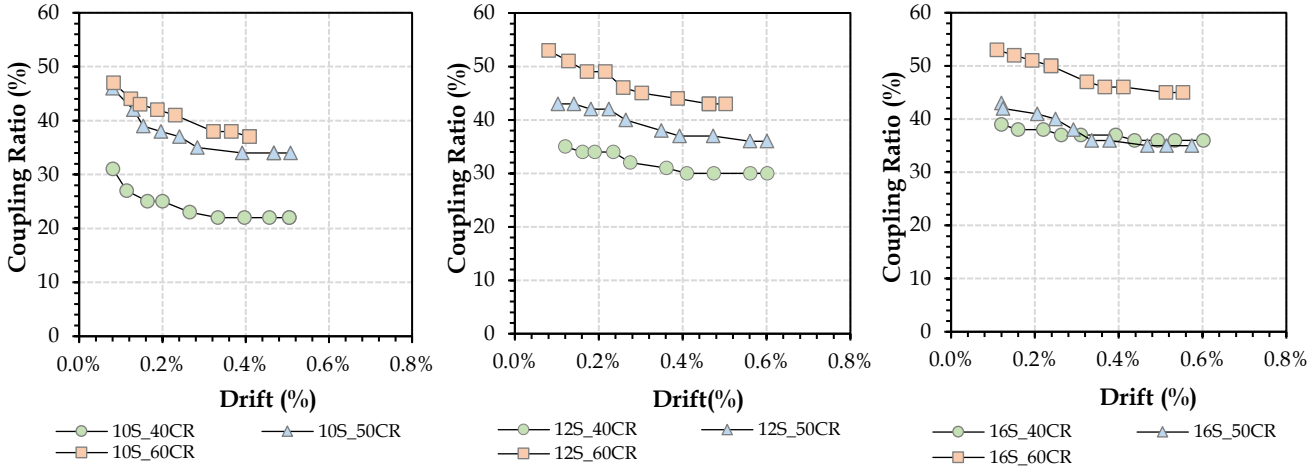

Fig 8. Variation in coupling ratio with increasing lateral drift

(e) Redistribution of Base Shear in Dual CSW-MRF system

The reduction in CR with increasing lateral drift demand (or PGA) leads to a corresponding decrease in the lateral translational stiffness of the CSW system (comprising the structural walls and coupling beams). This reduction subsequently lowers the overall lateral translational stiffness of the frame containing the CSW system (hereafter referred to as the CSW frame). As a result, the relative stiffness between the CSW frame and the parallel MRF frames changes with increasing PGA intensity. Consequently, the proportion of total base shear resisted by each subsystem differs with increasing PGA intensity. Specifically, the percentage of base shear resisted by the CSW frame decreases, while that resisted by the MRF frames increases, as illustrated in Fig 9. This redistribution implies that with increasing PGA intensity, the lateral force and displacement demand on the CSW frame reduce, whereas those on the MRF frames intensify. As a result, the MRF frames become more susceptible to damage due to the progressively higher force and deformation demands imposed on them.

Under low-intensity shaking (PGA = 0.16g), the CSW frame resists approximately 85% of the total base shear in the 10-storey buildings and about 72% in the 16-storey buildings. Correspondingly, the MRF frames resists only 15% and 28% of the total base shear, respectively. This indicates that at lower seismic intensities, the CSW frame primarily governs the lateral load and deformation resistance, as the coupling beams remain largely elastic and the overall lateral stiffness degradation of the CSW system is negligible. In contrast, at higher shaking intensities (PGA = 1.0g), the proportion of base shear resisted by the CSW frame decreases significantly—to about 44% for the 10-storey buildings and 8% for the 16-storey buildings. The MRF frames, therefore, resist 56% and 92% of the total base shear, respectively.

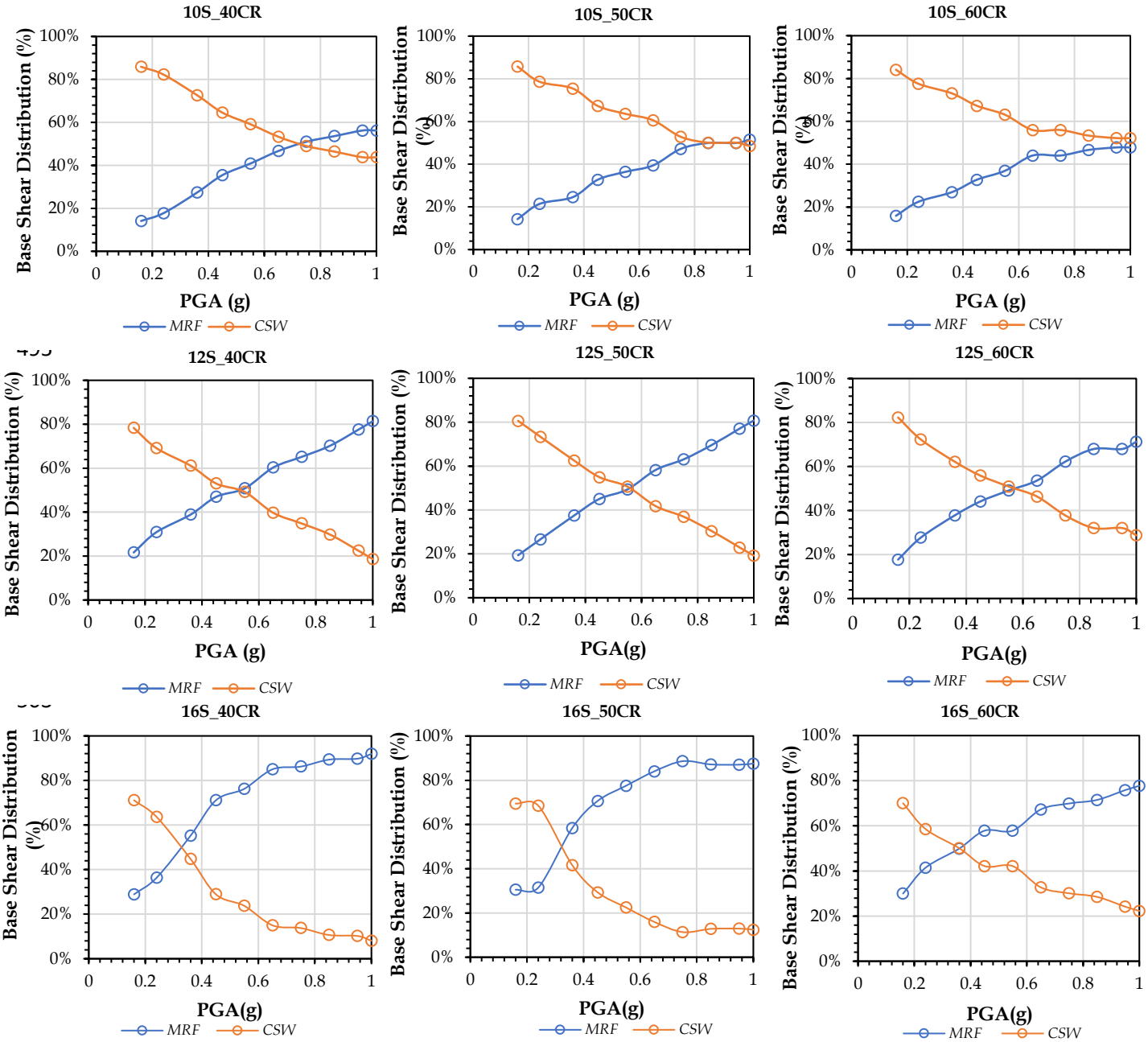

Fig 9. Redistribution of base shear demand to MRF and CSW system with increasing intensity of shaking

This substantial redistribution of seismic forces with increasing intensity highlights that, under strong shaking, the MRF frames assume a dominant role in lateral load resistance due to the degradation of coupling action and stiffness in the CSW frame. Design of MRF frame without due consideration to the possible increase in demand may lead to poor behaviour of dual CSW-MRF system. Again, this observation highlights the need to outline specific guidelines for the design of MRF part of dual CSW-MRF system.

Lastly, in addition to building height, the percentage of total base shear resisted by CSW frame and MRF frame varies with CR. For buildings of similar height (e.g., 16-storey buildings), adopting a higher CR (60%) results in a smaller redistribution of base shear from the CSW frame to the MRF frames with increasing seismic intensity. However, the overall extent of base shear redistribution is observed to be more sensitive to building height than to the CR, indicating that height plays a more dominant role in governing the relative stiffness degradation and load-sharing behavior between the CSW and MRF frames.

(f) Extent of damage in Dual CSW-MRF system

The study evaluates the damage in the dual CSW–MRF system using two parameters: (a) the extent of damage (discussed in this section) and (b) the degree of damage (presented in Section 3.2(g)). The term extent of damage for a given lateral drift demand is quantified using the percentage of hinge formation. This parameter is defined as the ratio of the number of beam flexural hinges that reach a specified damage state to the total number of potential beam hinge locations along the direction of loading. For instance, consider a system with ten beams spanning along X-direction, with two potential hinge locations per beam (one at each end), resulting in twenty possible hinge locations. If eight of these hinge locations exhibit yielding while the remaining twelve remain elastic at a given lateral drift demand (say 0.2%), the percentage hinge formation is 40% for yielding limit state (=8/20).

Furthermore, the study classifies beam damage into three distinct states—minor, moderate, and severe—as illustrated in Fig 10. A beam is considered to have reached a given damage state when its rotational demand, corresponding to a specific PGA intensity (or lateral drift demand), falls within the threshold limits defined in Table 6. The minor damage state represents limited structural damage to

the component. Likewise, moderate damage state represents significant structural damage to structural element. However, the damage to the element does not lead to local structural failure thereby ensuring life safety. Lastly, severe damage state represents severe damage to structural element. Structural element in this damage state could lead to local failure, which may lead to partial/total collapse of the building. In addition, three damage states, the study considers three categories of beams: coupling beams, intermediate beams, and normal beams, as illustrated in Fig 2. (a). The stepwise methodology to develop the extent of damage (along with an example) is listed in Table 7.

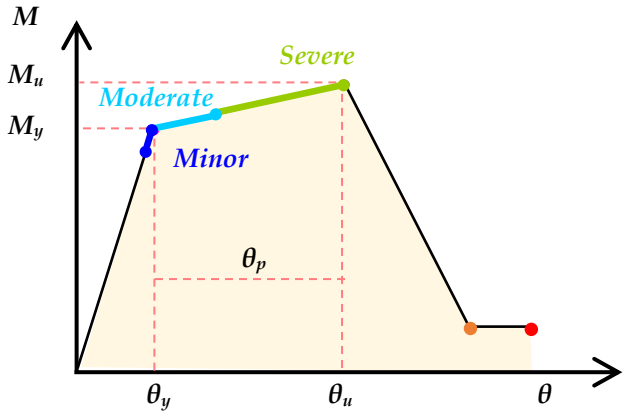

Fig 10. Various limit state defined for beams

Table 6. Damage state and the corresponding rotational threshold values

Damage State	Adopted Threshold
Minor Damage	Rotation exceeds $0.98\theta_y$
Moderate Damage	Rotation exceeds θ_y and is below $\theta_y + 0.25(\theta_u - \theta_y)$
Severe Damage	Rotation exceeds $\theta_y + 0.25(\theta_u - \theta_y)$ and is below $\theta_y + \theta_p$
θ_y Yield Rotation; θ_p Plastic Rotation; and θ_u Rotation corresponding to maximum flexural capacity	

Table 7. Stepwise methodology adopted to determine the extent of damage

Step	Details
Step 1	Estimate the total number of beams hinges along X-direction (say, 10-storey building). Additionally, identify the number of hinge in coupling beams (=40), intermediate beams (=60) and normal beams (=320).
Step 2	For a given PGA intensity (or corresponding lateral drift demand), the number of beam hinges reaching or exceeding the specified rotational thresholds is estimated. For instance, under a PGA of 0.75*g* for the 10S_40CR building, 306 hinges in the normal beams exceed the yield rotation, corresponding to a 96% hinge formation (=306/320). Under the same shaking intensity, 60 hinges in the intermediate beams exceed the yield rotation, resulting in a 100% hinge formation. Similarly, 40 hinges in the coupling beams exceed the yield rotation threshold. Notably, for all 40 hinge locations, the rotational demands fall within the range corresponding to moderate damage. Therefore, the percentage hinge formation for both minor and moderate damage states in the coupling beams is 100% (see Fig 11).

Fig. 11, 12 and 13 illustrates the extent of hinge formation in beams in 10-, 12-, and 16-strorey dual CSW-MRF system subjected to nonlinear static analysis with PGA levels ranging from 0.16g to 1g, respectively. In general, the building height and CR significantly influence the extent of hinge formation in beams. Among the different beam categories in all buildings, yielding (i.e., minor damage state) initiates first in coupling beams, followed by intermediate and normal beams. Again, for all buildings, compared to normal beams, intermediate beams exhibit a much faster progression towards 100% hinge formation for the minor damage state. This could be attributed to higher flexural stiffness of intermediate beam due to shorter span (=2m).

For the 10-storey CSW-MRF buildings, percentage hinge formation corresponding to the minor damage state initiates at relatively low PGA levels (approximately 0.16–0.45g) across all beam categories. Additionally, the rate of percentage hinge formation for this damage state is strongly influenced by the designed CR. For instance, in the case of normal beams, the percentage hinge formation corresponding to minor damage state in the 10S_40CR building reaches 100% at 0.85g, whereas in the 10S_60CR building it does not reach 100% even at 1g. This suggests that the normal beams do not participate significantly in energy dissipation when buildings are designed considering higher CR values. Thus, designing for higher CR could ensure limited damage to normal beams ensuring continuous functionality of the system as a whole.

Among different beam categories, coupling beams exhibits the fastest progression towards 100% hinge formation for minor (=0.36g) and moderate damage state (=1g) in 10-storey CSW-MRF buildings. Additionally, coupling beams in 10S_40CR reaches 100% hinge formation corresponding to moderate damage state sooner (=0.75g) than 10S_60CR (=1g). This qualitatively indicates that the plastic rotation demand in coupling beams present in 10S_40CR to be higher than the same present in 10S_60R due to early formation of hinges. In summary, it is evident that the energy dissipation is predominantly driven by inelastic action in coupling beams.

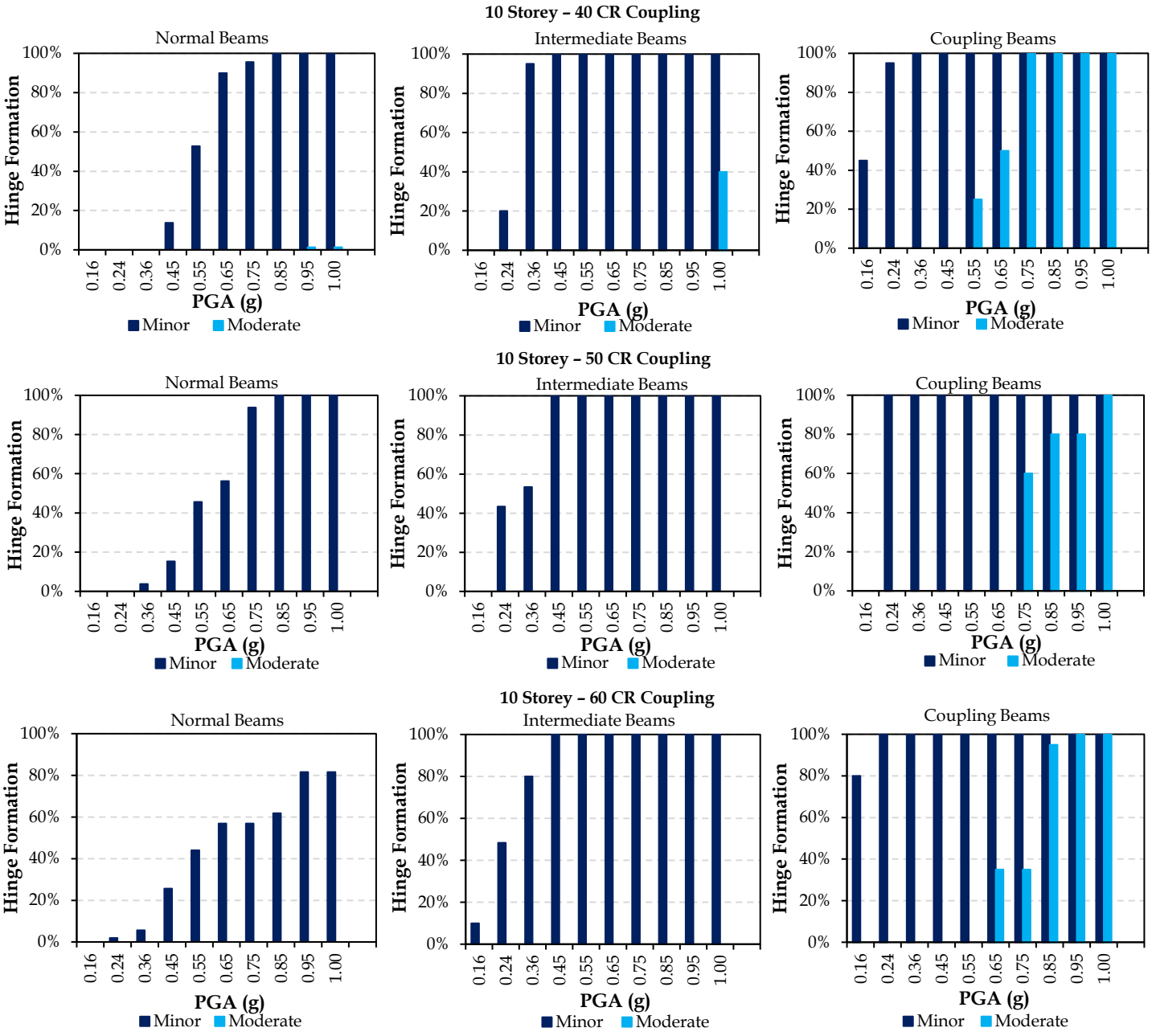

Fig 11. Formation of hinges for 10-storey building with 40CR, 50 CR and 60 CR coupling ratio

In general, the 12-storey CSW-MRF buildings exhibited a hinge development pattern similar to that of the 10-storey buildings, albeit with a slightly delayed initiation. This delay can be attributed to the reduced lateral stiffness associated with the increased building height. Normal beams displayed minimal hinge formation below 0.36*g*, with a gradual increase beyond 0.55*g*, ultimately reaching at least 90% hinge formation corresponding to the minor damage state at 1.0*g*. Consistent with the 10-storey systems, coupling beams remained the primary energy-dissipating elements across all coupling ratios, exhibiting 100% hinge formation for the minor damage state at 0.36*g* and over 90% hinge formation for the moderate damage state at 1.0*g*. Overall, compared with the 10-storey buildings, the 12-storey configurations demonstrated a lower proportion of hinges corresponding to the moderate damage state, indicating relatively reduced inelastic demand in taller systems.

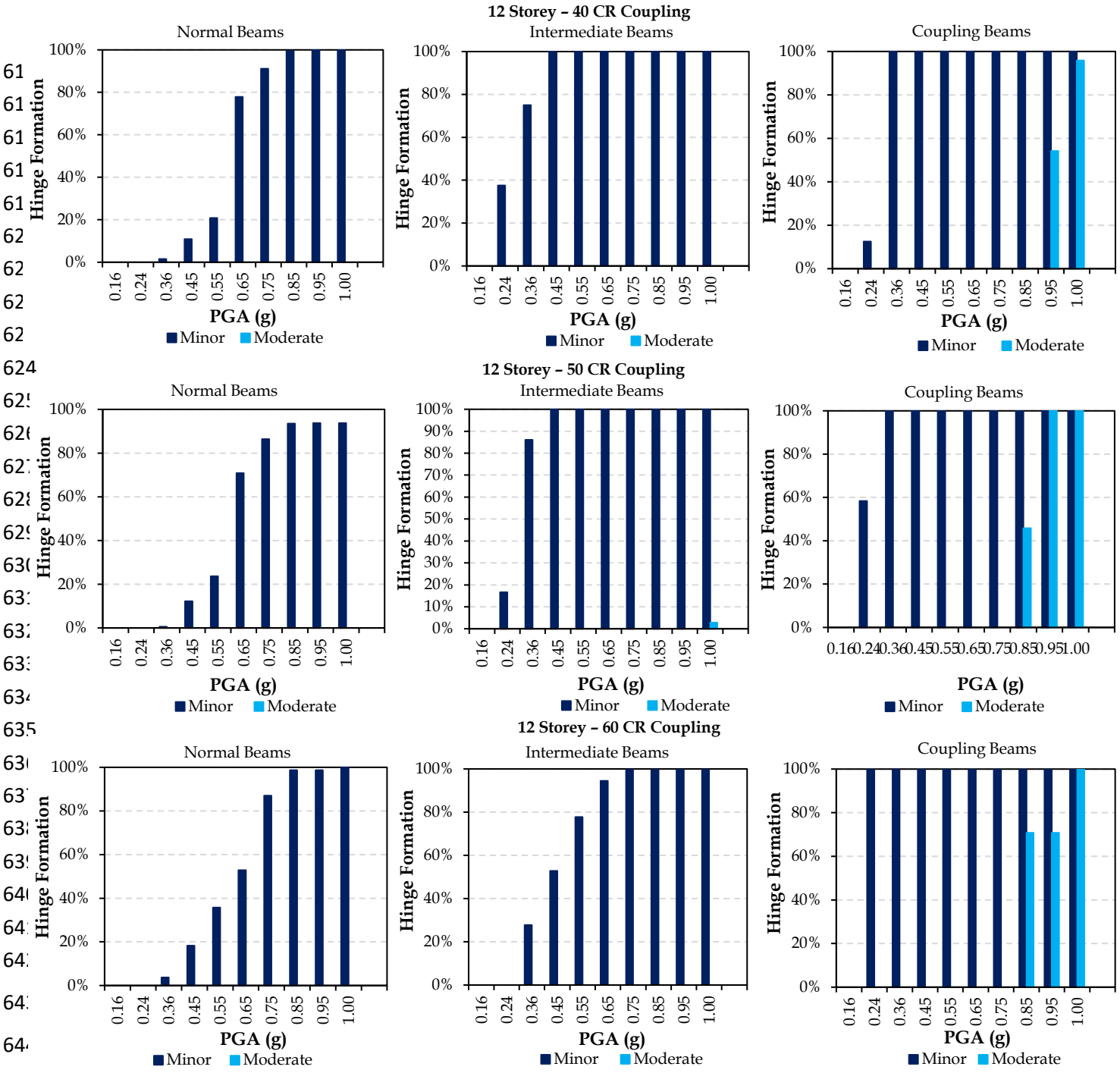

Fig 12. Formation of hinges for 12-storey building with 40CR, 50 CR and 60 CR coupling ratio

Among all configurations, the 16-storey CSW-MRF buildings exhibited the slowest rate of hinge formation corresponding to both the minor and moderate damage states across all beam categories. The onset of damage was also delayed for both damage states, which can be attributed to the reduced lateral translational stiffness associated with increased building height. Across all beam categories, the initiation of minor damage hinges occurred first in the coupling beams, followed by the intermediate and normal beams, consistent with the behavior observed in shorter buildings. Notably, unlike the 10-storey systems, the percentage of hinges corresponding to the moderate damage state in the 16-storey

653 CSW-MRF buildings was highest for the 60CR configuration and lowest for the 40CR configuration.
654 This trend suggests that adopting a lower coupling ratio (CR) in taller buildings helps limit damage in
655 coupling beams. This behavior is expected, as a lower CR imparts greater overall flexibility, enabling
656 the structure to accommodate seismic demand more elastically—thereby reducing inelastic
657 deformation demands in the coupling beams.

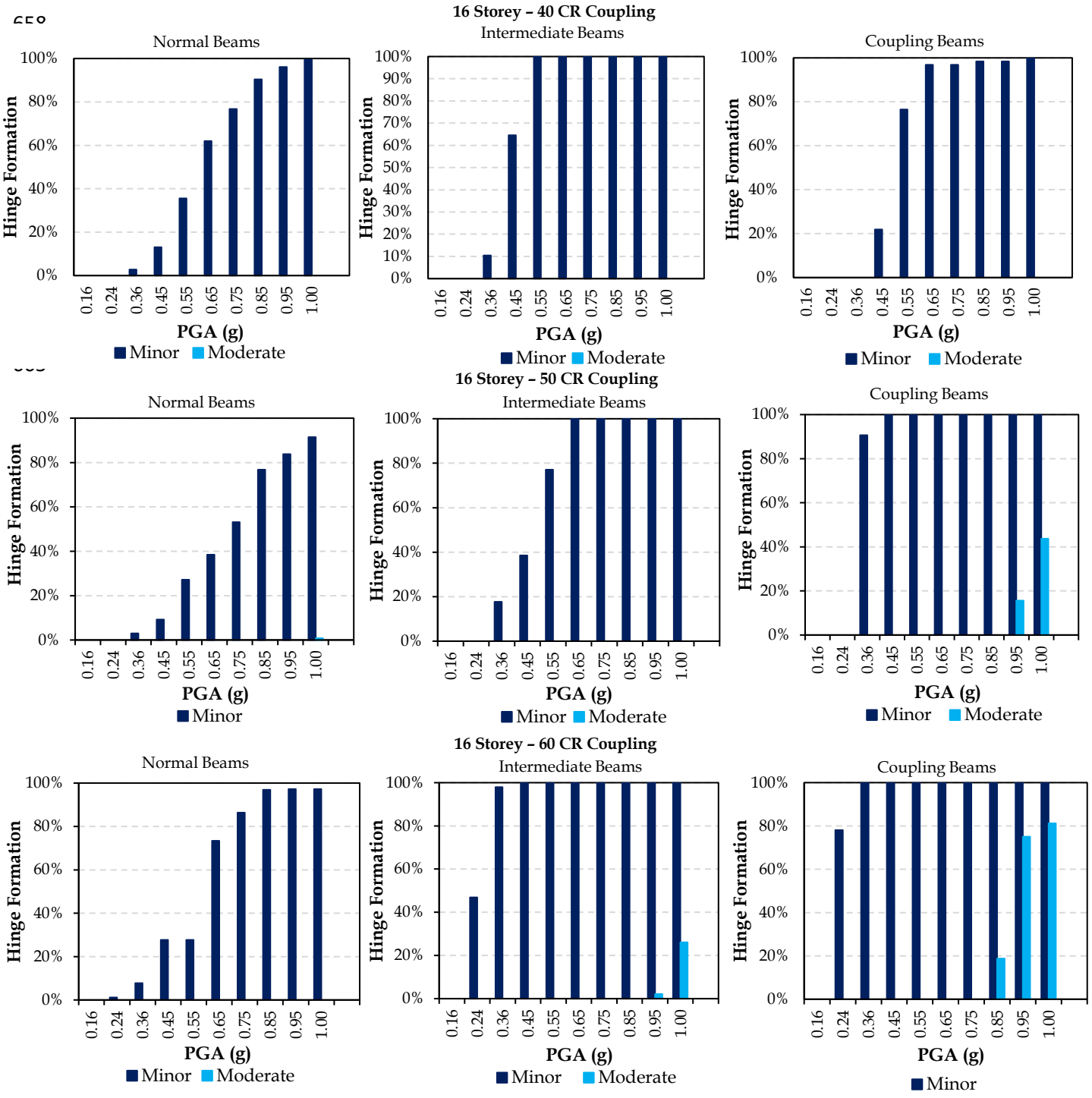

680 **Fig 13.** Formation of hinges for 12-storey building with 40CR, 50 CR and 60 CR coupling ratio

(*g*) ***Degree of damage in Dual CSW-MRF system***

The degree of damage represents the maximum plastic rotation demand experienced by different structural elements at varying PGA levels. To better interpret the distribution of plastic rotation demands in beams, the beam damage is classified into two categories: (i) localized damage and (ii) non-localized damage. Localized damage refers to the plastic rotation demand in beams that frame into structural walls (part of the CSW system), while non-localized damage refers to that in beams framing into columns (part of the MRF system). By definition, coupling beams are classified as exhibiting localized damage, whereas intermediate beams, which are part of the moment frame, exhibit non-localized damage. In the case of normal beams, some frame into the structural walls (contributing to localized damage), while others frame into columns (contributing to non-localized damage), as illustrated in Fig 2. (a). This distinction is made because existing literature [50] indicates that beams framing into structural walls experience higher plastic rotation demands than those framing into columns, owing to the greater concentration of inelastic action near wall–beam interfaces [51].

Fig 14. illustrates the degree of damage (i.e., plastic rotation demand) in beams with peak ground acceleration (PGA) for all dual CSW-MRF buildings. In general, plastic rotation demand is observed to increase nonlinearly with PGA. Additionally, the plastic rotation demand appears to increase gradually up to a PGA of 0.4*g* thereafter increasing sharply to reach the maximum value at 1*g*. This behavior reflects the transition from elastic to inelastic response as seismic intensity increases. The trend is consistent across all building heights and coupling ratios, signifying that PGA imposes greater inelastic deformation demands on the structural elements.

The influence of CR is generally modest across beam types and building heights. For normal beams, changes in CR have limited impact on plastic rotation demand, suggesting lesser sensitivity to coupling ratio. In contrast, coupling beams exhibit slightly higher plastic rotation demands with increasing CR, especially at higher PGA levels, due to higher stiffness and interaction between coupled walls. For non-localized damage (intermediate and normal beams framing into columns), variations across coupling ratios remain minimal, implying that the overall global performance of the dual system is relatively insensitive to moderate changes in coupling ratio.

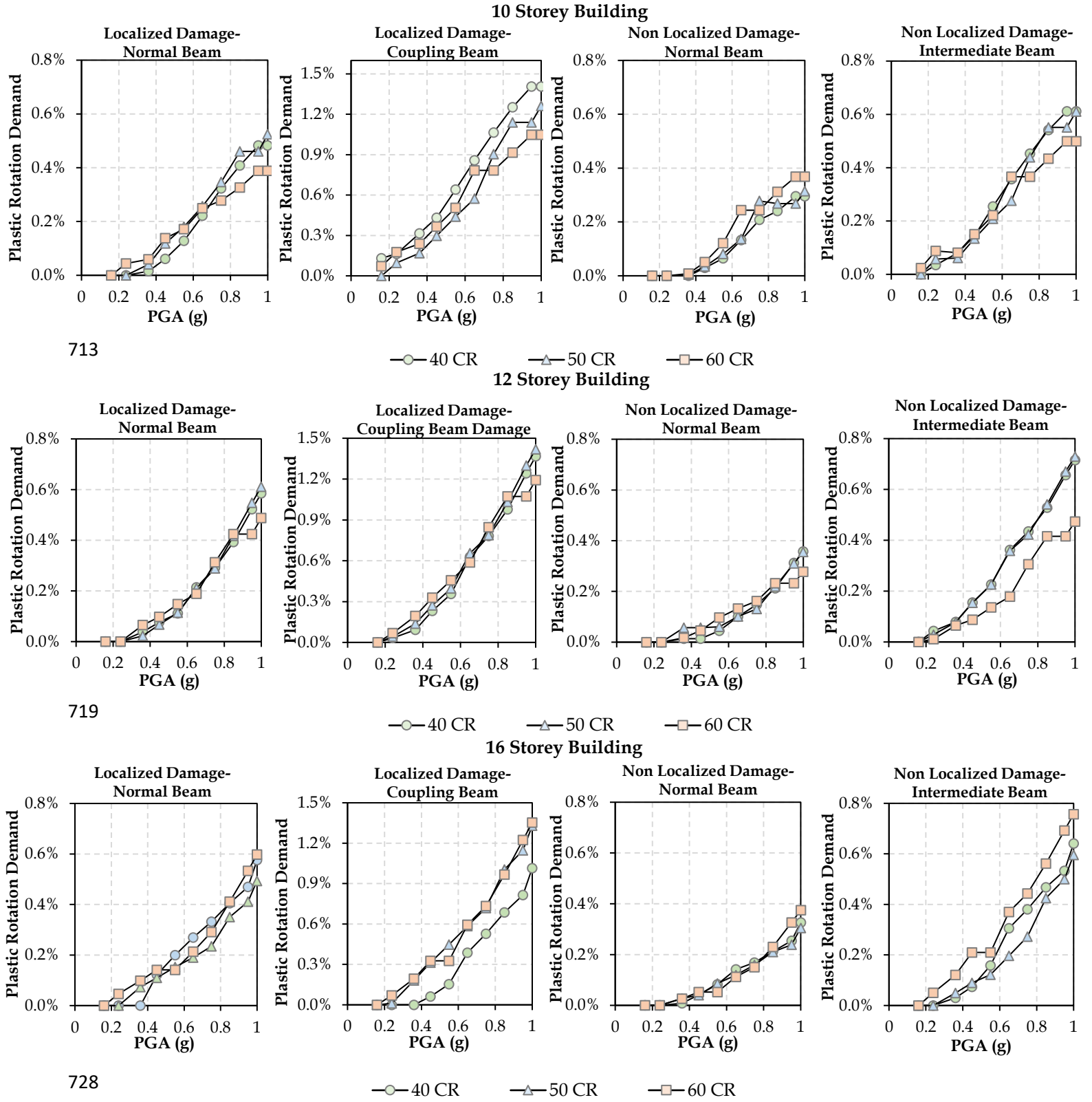

Fig 14. Plastic rotation demand in beams

In terms of structural height, taller buildings (e.g., 16-storey) show lower plastic rotation demands compared to shorter buildings under similar PGA levels. This reduction is attributed to the longer fundamental periods of taller buildings, which result in lower acceleration and drift demands. Additionally, localized damage, particularly in coupling beams, consistently exhibits higher plastic

734 rotation demands than non-localized damage, emphasizing the dominant role of coupling beams in the
735 inelastic response of CSW-MRF buildings.

736 Fig 15. illustrates the plastic rotation demand in columns. Similar to beams, damage to columns that
737 are part of CSW frame system is categorized as localized damage. Damage to columns that are part of
738 MRF system is categorized as non-localized damage. In general, the plastic rotation demands in
739 columns are significantly smaller compared to the same in beams. This indicates that the columns
740 remain nearly elastic even for strong earthquake shaking of 1*g*. Moreover, the variation of CR and
741 building height exhibits no significant difference on the plastic rotation demands in columns. This
742 indicates that the plastic rotation demand in columns is independent of CR and building height.

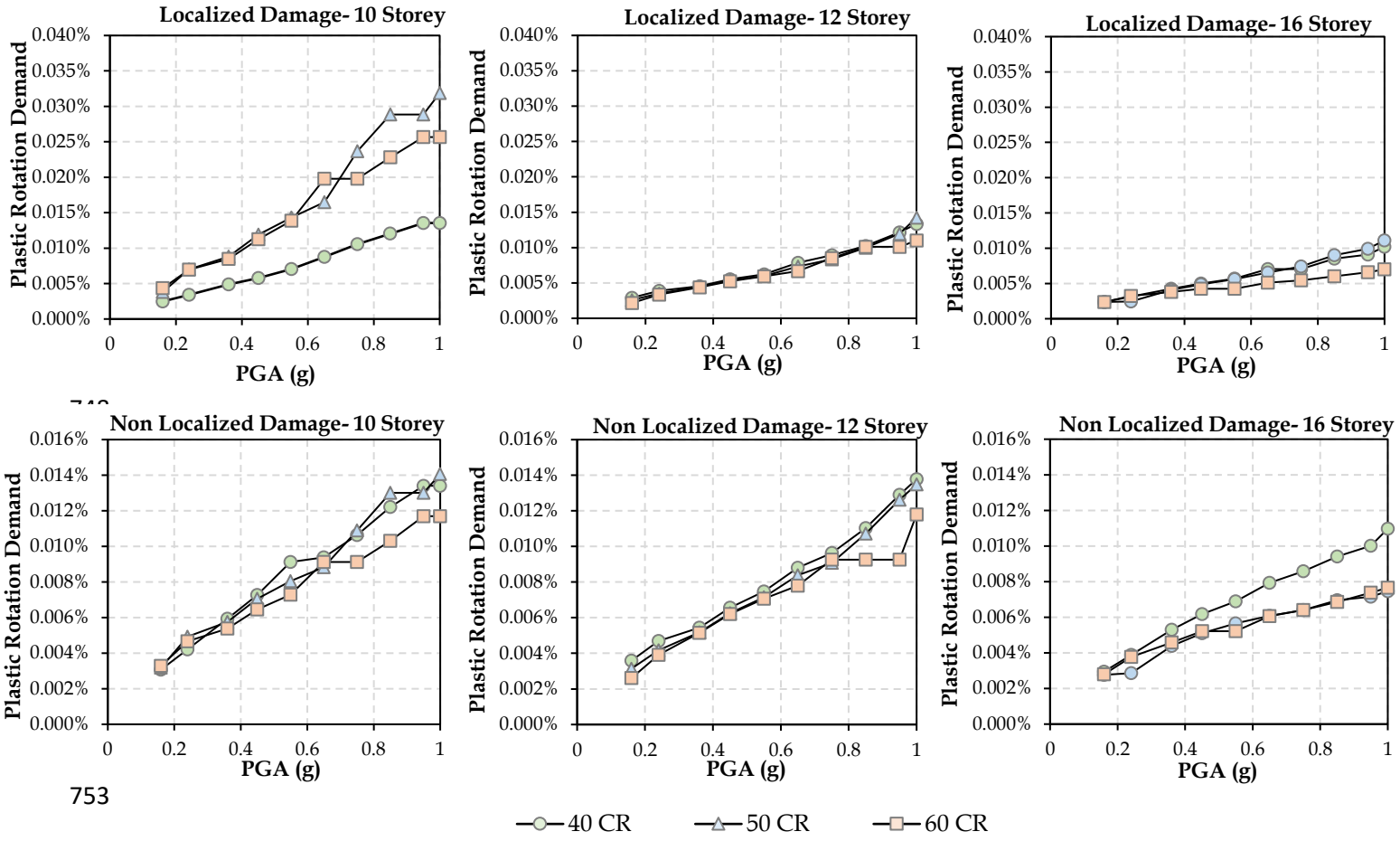

753

754 **Fig 15.** Plastic rotation demand in columns

755

756

Lastly, Fig 16. illustrates the variation of plastic rotation demand in structural walls with PGA. The plastic rotation demands in structural walls are significantly lesser than that for coupling beams and localized normal beams. This indicates that the coupling beam predominantly influences the energy dissipation in dual CSW-MRF buildings. However, the plastic rotation demand in structural walls, in general, is comparable to the plastic rotation demand in non-localized normal beams. With the exception of 16-storey buildings, the variation of CR does not lead to significant change in the plastic rotational demand in structural walls. Furthermore, for both 10- and 12-storey buildings, the plastic rotation demand in structural wall appears to be similar in magnitude.

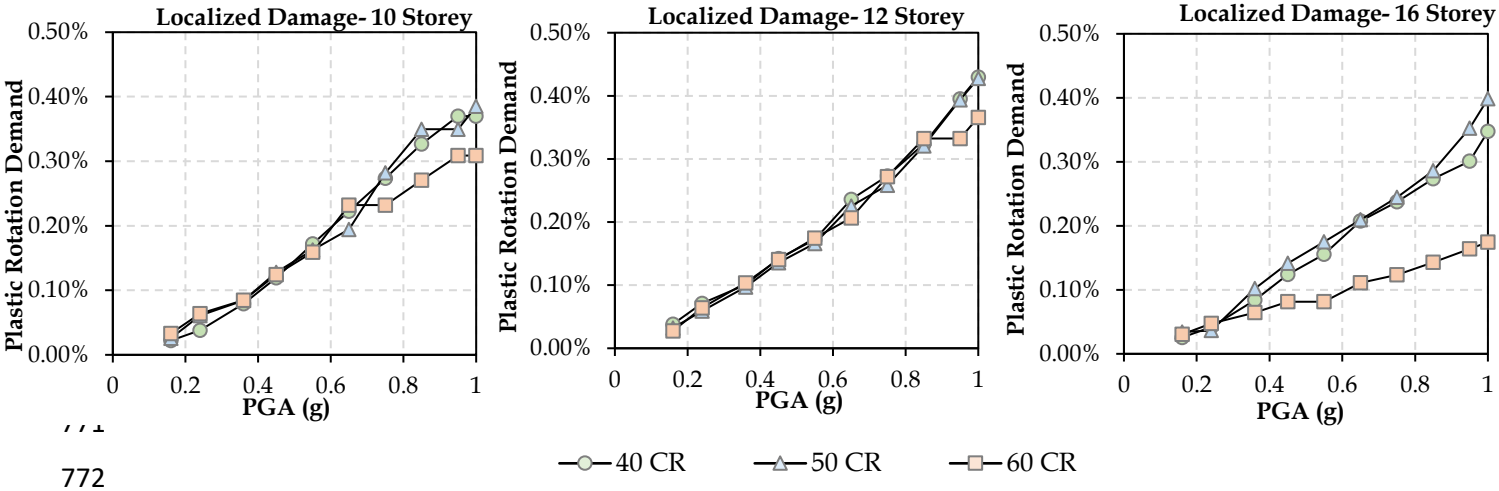

Fig 16. Plastic rotation demand in structural walls

(h) Probable Loss Estimate for Dual CSW-MRF system

A loss function, often denoted as $L(I,T)$, represents a function that depends on seismic intensity (I) and recovery time (T). The said function is used to evaluate seismic damage by estimating losses resulting from earthquakes. Losses, in general, are categorized into two types; namely, direct and indirect economic losses. Direct economic losses pertain to damages to the structural and non-structural elements present in the buildings, while indirect economic losses are time-sensitive and include costs such as relocation, revenue loss, price increases, and related expenses. The loss function combines probabilistic damage estimates with associated costs, offering a comprehensive assessment of the financial impacts of an earthquake. This can aid in developing strategies to mitigate financial losses, ultimately enhancing the resilience of communities and infrastructure.

In this study, only the direct loss pertaining to damage to structural elements is quantified and economic impact is analyzed using pushover analysis. Damage to non-structural elements is not considered in this study. The loss estimates for the nine archetype buildings were quantified using the three defined damage states defined in section 3.2(f). The probability of exceedance of each damage states at the performance point was determined for different PGA levels, ranging from 0.16g to 1.0g. The direct loss was calculated using the formula outlined in the HAZUS MR4 manual [52], as follows:

$$\text{Direct Economic Loss Function, } \quad L_D = \sum P_E(DS = K) \times r_k \tag{1}$$

where, $P_E(DS = K)$ is the discreet damage probability in damage state (DS); K the damage state of the building (as defined in Table 6) and r_k is the damage ratio corresponding to damage state (DS). The $P_E(DS = K)$ of a damage state (say, *minor*) was evaluated as the ratio of the number of beams that attained the predefined limit state (minor) to the total number of beams in the building. The r_k corresponding to various damage states of the building were adopted from the HAZUS manual [52]. The value of damage ratio (r_k) for different damage levels adopted in this study are listed in Table 7.

Table 8. Damage ratio considered in this study

Damage States	*Minor*	*Moderate*	*Severe*
r_k	0.10	0.40	1.00

Fig 17. illustrates the variation in probable loss estimate with increase in lateral displacement demand (or PGA intensity). The loss percentage, in general, exhibits a nonlinear trend. For 10-storey CSW-MRF buildings, the losses increase linearly from 1 to 2% (at 0.16g) to 16% (at 1g). Moreover, among the 10-storey buildings, 10S_40CR indicates a consistently higher loss compared to buildings designed using either 50CR or 60CR. The trend observed for 12-storey CSW-MRF buildings are similar to that for 10-storey buildings. However, the losses for 12-storey buildings are marginally lower than that for 10-storey buildings. For 12-storey buildings, the loss percentage is around 4 to 5% at 0.5g and around 13 to 14% at 1g. For 12-storey buildings, CR does not significantly influence the variation in loss percentage. For 16-storey buildings, the loss percentage is about 5 to 6% at 0.6g and around 10 to 14% at 1g. 16S_60CR exhibits the highest loss among 16-storey buildings. In summary, the loss percentage appears to mirror the behavior observed in the extent and degree of damage to structural elements.

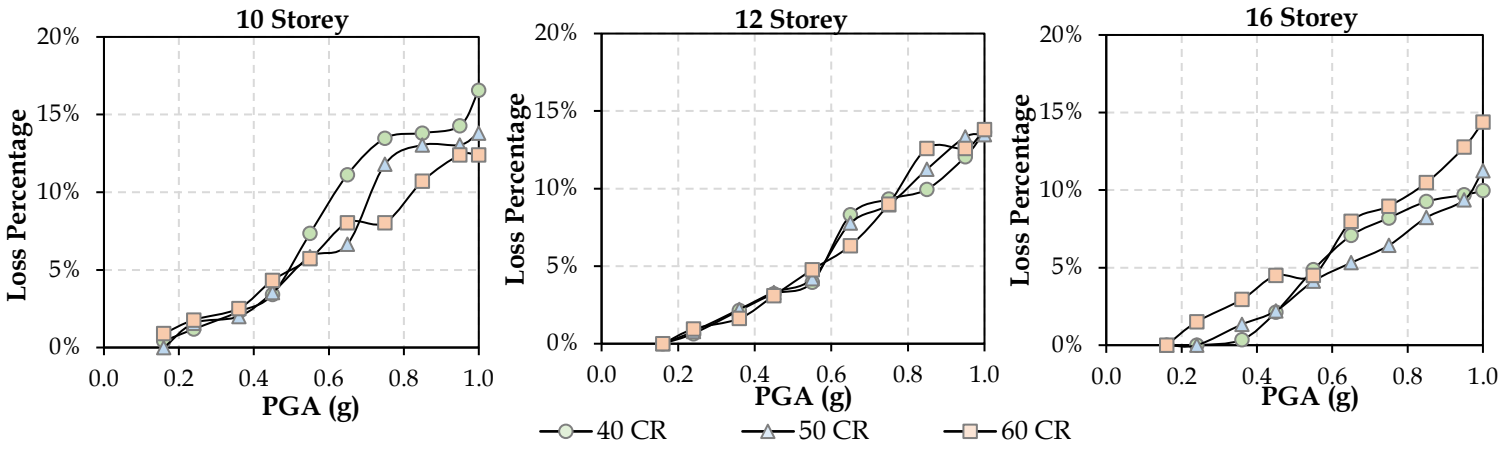

Fig 17. Probable loss estimate of buildings based on damage states

(i) Functional Recovery for Dual CSW-MRF system

Seismic resilience refers to a structure's ability to recover and restore functionality after an earthquake event over a period defined as the control time *Q(t)*. Resilience is generally measured in terms of either static resilience (i.e., robustness) or dynamic resilience (i.e., rapidity) [53]. The former refers to the system's ability to minimize maximum impact. The latter refers to how quickly the system recovers from a disruption. The key characteristics of resilience of a structure are *rapidity, robustness, redundancy* and *resourcefulness* [54]. Generally, the seismic resilience for a building is quantified as an index, and is expressed as a number between 0 and 100% (Fig 18.).

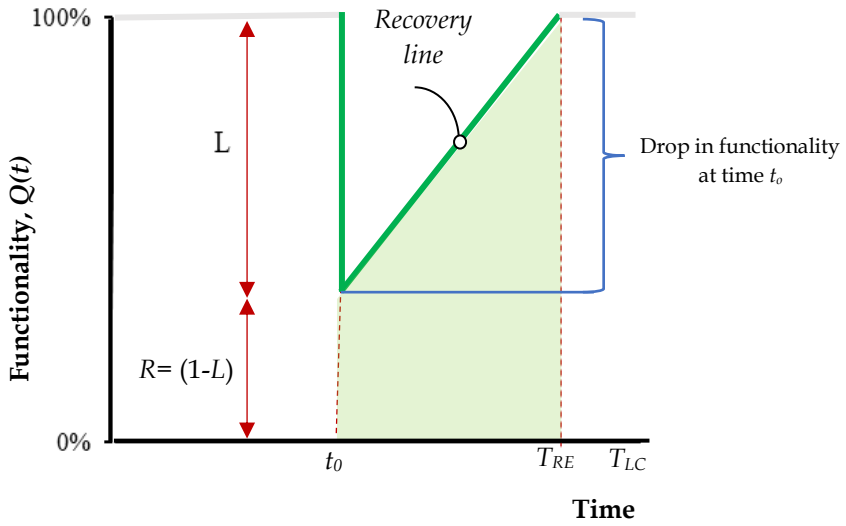

Fig 18. Seismic resilience curve based on functionality [55]

In Fig 18, the area under the recovery line (encompassed between time t_0 and T_{RE}) represents the resilience of the system. In the above illustration, the parameter $t_{0,}$ refers to the time of disruption (i.e., loss in building functionality due to damage to structural elements). Likewise, the parameter T_{RE} refers to the time required to restore full functionality of the building after the disruptive event (i.e., the time

required to repair/retrofit structural elements). This rate of dip in functionality depends on several factors including the type of hazards, preparedness of the structural system, location of the incident, and availability of resources. For a single event, resilience can be mathematically expressed as:

$$R = \int_{t_{oE}}^{t_{oE}+T_{Lc}} \frac{Q(t)}{T_{Lc}dt} \tag{2}$$

$$Q(t) = [1 - L(I, T_{RE})][H(t - t_{oE}) - H(t_{oE} + T_{RE})][f_{\mathrm{Rec}}(t, t_{oE}, t_{RE})] \tag{3}$$

where t_{oE} is the time of occurrence of event, T_{LC} control time of the system E, $L(I,T_{RE})$ loss function; $H()$ Heaviside step function, f_{Rec} (t, t_{0E}, T_{RE}) is the recovery function, and T_{RE} recovery time from event E necessary to reach pre-disaster state. $Q(t)$ is a percentage that changes over time, and resilience can be shown graphically as the shaded area below functionality function of a system (i.e., recovery line), (Fig 18).

Assessing the seismic resilience of a structure involves evaluating the recovery functions. The rapid functionality of a structure depends on the recovery functions and should be chosen based on community preparedness and structural response [56-60]. In general, three recovery functions are used, *i.e.,* linear recovery function, exponential recovery function, and trigonometric recovery function. In this study, it is assumed that the services will be available in a timely manner and functionality can be achieved readily. Hence, the study considers a linear recovery functions to assess the seismic resilience of dual CSW-MRF buildings. The linear recovery function is computing as follows:

$$f_{recovery}(t, t_{oE}, T_{RE}) = \left[1 - \frac{t - t_{oE}}{T_{RE}}\right] \tag{4}$$

where, t_{oE} is the time of occurrence of the seismic event and T_{RE} is the recovery time of the structure to return back to its target functionality. Since no specific guidelines exist in Indian standards for estimating recovery functions, the study adopts approaches from existing literature to evaluate the resilience of existing and newly designed buildings under various levels of PGA, using predefined time intervals for recovery [60,61]. For the study, control time (TLC) of 140 days and control time of 50 days was considered. For the study, control time (T_{LC}) of 140 days and control time of 50 days was pre-assumed. The initial recovery time (T_{RE}) for 40 CR building was taken as 65 days, and the slope of the

function was taken as the recovery time for 50 CR and 60 CR buildings. The target functionality level was assumed to attain on the 120th day. Using Eqn. (4**)** the building's functionality was determined with pre-disaster incident measured at a target functionality level of 100 percent. The functionality curves were plotted against the loss in functionality (%) and time(t) for PGA level corresponding to 1g, using linear recovery function.

Fig 19. illustrates the recovery trajectory of the study buildings following an earthquake with a PGA of 1.0g. Among the 10-storey buildings, 10S_40CR building exhibited the least seismic resilience, with its post-earthquake functionality reducing to 83% due to extensive damage sustained by the coupling beams (as shown in Fig 11. and Fig 14.). In comparison, 10S_50CR and 10S_60CR demonstrated slightly improved functionality levels of 86% and 88%, respectively. A similar trend was observed for the 12-storey buildings, where the post-event functionality ranged between 86% and 88% across all CRs. Among the 16-storey buildings, 16S_60CR building exhibited the least seismic resilience, with functionality dropping to 86%, followed by 16S_50CR (88%) and 16S_40CR (90%). Overall, the results indicate that a higher CR tends to marginally enhance seismic resilience and functionality recovery for 10- and 12-storey buildings.

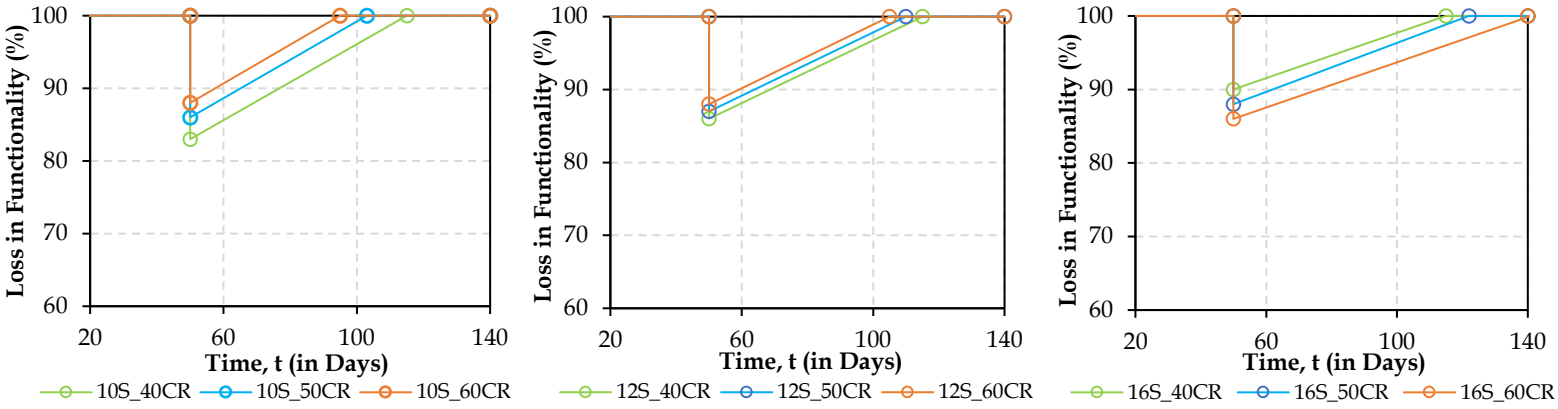

Fig 19. Recovery path of buildings using linear function

4. Summary & Conclusion

The objectives of the study are as follows: (a) quantify the increased lateral force demand (i.e., base shear demand) in MRFs resulting from redistribution of forces with progressive damage to coupling beams in CSW system, (b) recommend column design capacities required to preclude shear failure in structural members part of MRFs, and (c) evaluate the seismic performance of dual CSW–MRF system, including resilience assessment in terms of probable loss estimates and functional recovery. For this

purpose, nine buildings of different heights (10-, 12- and 16-storey) and three different coupling ratios (40CR, 50CR and 60CR) were considered. The seismic performance of the study buildings is quantified using nonlinear static analysis.

The salient *conclusions* drawn from the study are:

1. It is necessary to design columns (that are part of moment resisting frames) with a minimum shear capacity that equals 50% of maximum shear capacity of the column. This is necessary to preclude shear failure of the column, which could detrimentally reduce the lateral displacement capacity of the dual CSW-MRF buildings.

2. The dual CSW–MRF system with increased nominal column shear capacity exhibited a lateral displacement capacity approximately 2.27 times greater than that designed with the IS 13920:2016-based shear capacity.

3. For buildings with similar height, those designed with higher CR indicate an increase in: (a) lateral translational stiffness (K) (by 22-52%); and (b) ultimate strength (by 6-15%).

4. In general, for buildings designed with higher CR, the ultimate drift capacity (Δ_u) of the dual CSW-MRF building is reduced by 6–38%. In addition, the displacement drift demand is also reduced for buildings designed with higher CR (owing to higher initial stiffness).

5. When buildings are subjected to increasing lateral drift demand, the damage to coupling beams leads to a reduction in CR. Additionally, the rate of reduction in 16-storey building is observed to be smaller than that for 10-storey building.

6. When lateral drift demand corresponding to a PGA of 0.16g was imposed on the dual CSW-MRF building, the CSW frame resisted approximately 85% of the total base shear in 10-storey buildings and 72% in 16-storey buildings. However, when lateral drift demand corresponding to a PGA of 1.0g was imposed on the dual CSW-MRF building, the CSW fame's base shear resistance reduced drastically to 44% and 8%, respectively. This highlights the significant redistribution of base shear demand between the CSW frame and the MRF frame.

7. In general, with the increase in design CR, the onset of hinge formation is delayed leading to reduced plastic rotation demand in buildings with higher CR, with the exception of 16S_40CR. In addition to CR, the building height is one of the contributing factors towards the hinge formation and plastic rotation demand in dual CSW-MRF buildings.

8. Among all energy dissipating elements in dual CSW-MRF buildings, coupling beams resist the maximum plastic rotation demand in the range of 1 to 1.4% (i.e., 0.01 to 0.014 radians) while sustaining a PGA of 1g. Additionally, as expected, the beams framing into the structural walls have higher rotational demand (i.e., localised damage) compared to the same for beams framing into columns that are part of MRF.

9. The probable loss percentage increases nonlinearly with PGA. Relative to CR, building height appears to significantly influence the probable loss estimate. For instance, the loss estimate reaches about 16% at 1g for 10-storey, 13–14% for 12-storey, and 10–14% for 16-storey dual CSW-MRF buildings.

Notwithstanding the limited number of building configurations investigated in this study, the following recommendations are proposed for consideration in the seismic design of dual CSW–MRF buildings: (a) columns part of MRF system should be provided with a minimum shear capacity of not less than 50% of their maximum shear strength to mitigate the risk of premature shear failure; and (b) the CSW may be proportioned with a CR of approximately 50% to achieve a balanced increase in lateral stiffness, lateral strength, deformation capacity, and post-earthquake functional recovery of the overall system.

While the present study primarily examines the influence of coupling ratio (CR) and building height on the seismic resilience of dual CSW-MRF systems, certain aspects merit further investigation. The influence of centrally located coupled structural walls, typically incorporated around stairwells and elevator cores, warrants further investigation. Additionally, the grouping of coupling beams during the design stage and the adoption of alternative lateral load distributions during analysis could provide additional insights into the building's seismic performance. Furthermore, the assumed recovery period of 65 days, used in computing seismic resilience, represents an idealized estimate and may vary under

practical post-earthquake conditions; hence, sensitivity analyses considering variable recovery durations are recommended.

The current assessment also excludes losses associated with non-structural components, which recent seismic events have shown to significantly affect overall functionality and recovery. Future studies should therefore incorporate these effects to achieve a more comprehensive evaluation of resilience. Finally, as the findings presented herein are based on a limited number of representative building models, further analyses involving a broader set of dual CSW-MRF configurations subjected to nonlinear time-history simulations are required to establish generalized design recommendations, particularly for the moment frame columns.

5. Acknowledgement

The first author gratefully acknowledges the financial support received under the Savitribai Jyotirao Phule Fellowship awarded by the University Grants Commission (UGC), India. Furthermore, the first author acknowledges the financial assistance received under the Erasmus ICM Program, funded by the European Commission, in collaboration with Amrita Vishwa Vidyapeetham, India and University of Trento, Italy, which facilitated the completion of this work. Additionally, the third author gratefully acknowledges the support of the Director, CSIR-SERC, for enabling this collaborative work and the registration number "CSIR-SERC 1374/2025" has been assigned to the paper by CSIR-SERC for traceability. The views and opinions expressed in this paper are solely those of the authors and do not necessarily reflect those of the affiliated institutions or funding agencies.

Annex A

Table A1. Reinforcement details of study buildings (Member sizes are available in Table 1)

Building	*Members*	*Longitudinal Reinforcement Details (%)*		*Shear Reinforcement (%)*
		Top	*Bottom*	
C10_40	Beam	*0.33%-0.87%*	*0.33%-0.45%*	*NB-2L-8mmϕ@200mm* *IB-2L-10mmϕ@150mm* *CB-2L-8mmϕ@150mm*
	Column	*0.85%*		*3L-10mmϕ@150mm*
	Structural Wall	*2.44%*		*2L-12mmϕ@150mm*
C10_50	Beam	*0.34%-1.36%*	*0.34%-1.36%*	*NB-2L-10mmϕ@100mm* *IB-2L-8mmϕ@100mm* *CB-2L-8mmϕ@100mm*
	Column	*0.85%*		*3L-10mmϕ@150mm*
	Structural Wall	*2.44%*		*2L-12mmϕ@150mm*
C10_60	Beam	*0.34%-1.47%*	*0.33%-0.87%*	*NB-2L-10mmϕ@100mm* *IB-2L-8mmϕ@150mm* *CB-2L-8mmϕ@100mm*
	Column	*0.85%*		*3L-10mmϕ@150mm*
	Structural Wall	*2.44%*		*2L-12mmϕ@150mm*
C12_40	Beam	*0.33%-1.47%*	*0.33%-1.31%*	*NB-2L-10mmϕ@100mm* *IB-2L-10mmϕ@100mm* *CB-2L-10mmϕ@100mm*
	Column	*1.18-4.19%*		*3L-12mmϕ@150mm*
	Structural Wall	*2.44%*		*3L-12mmϕ@120mm*
C12_50	Beam	*0.33%-1.74%*	*0.33%-1.58%*	*NB-2L-10mmϕ@100mm* *IB-2L-10mmϕ@100mm* *CB-2L-8mmϕ@100mm*
	Column	*1.18-4.19%*		*3L-12mmϕ@150mm*
	Structural Wall	*2.44%*		*2L-12mmϕ@120mm*
C12_60	Beam	*0.33%-1.74%*	*0.33%-1.64%*	*NB-2L-10mmϕ@100mm* *IB-2L-8mmϕ@100mm* *CB-2L-8mmϕ@100mm*
	Column	*1.18-4.19%*		*3L-12mmϕ@150mm*
	Structural Wall	*2.44%*		*2L-12mmϕ@120mm*
C16_40	Beam	*0.42%-2.05%*	*0.38%-1.69%*	*NB-2L-10mmϕ@120mm* *IB-2L-8mmϕ@150mm* *CB-2L-8mmϕ@120mm*
	Column	*1.18-4.19%*		*3L-12mmϕ@150mm*
	Structural Wall	*3.01%*		*3L-12mmϕ@120mm*
C16_50	Beam	*0.42%-2.05%*	*0.38%-1.69%*	*NB-2L-10mmϕ@120mm* *IB-2L-8mmϕ@150mm* *CB-2L-8mmϕ@120mm*
	Column	*1.18-4.19%*		*3L-12mmϕ@150mm*
	Structural Wall	*3.01%*		*2L-12mmϕ@120mm*
C16_60	Beam	*0.33%-2.12%*	*0.33%-1.98%*	*NB-2L-10mmϕ@100mm* *IB-2L-8mmϕ@150mm* *CB-2L-8mmϕ@120mm*
	Column	*1.18-4.19%*		*3L-12mmϕ@150mm*
	Structural Wall	*3.01%*		*2L-12mmϕ@120mm*

976 **A1. Detailing of Beams**

Building Details	Normal Beams	Intermediate Beams	Coupling Beams
10S_40CR	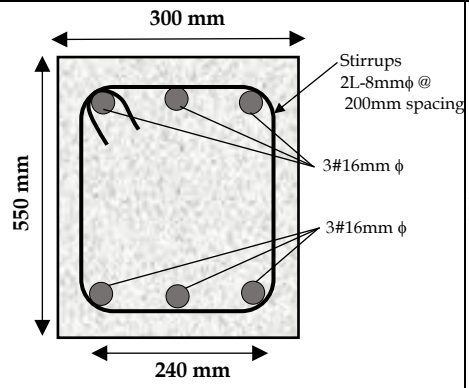	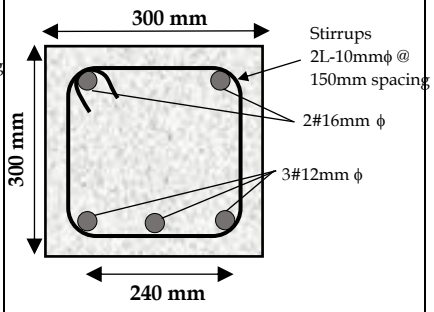	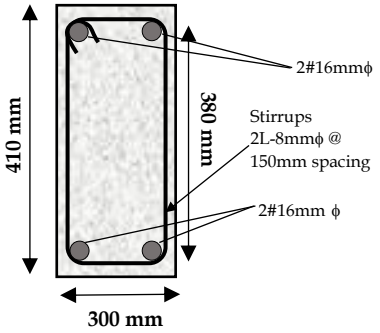
10S_50CR	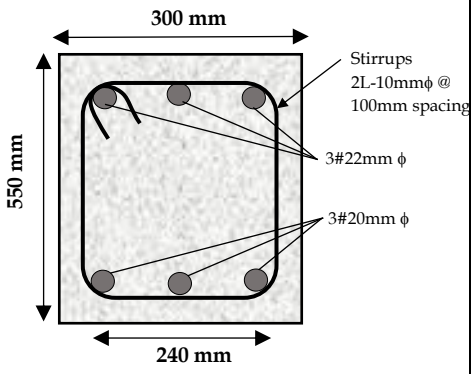	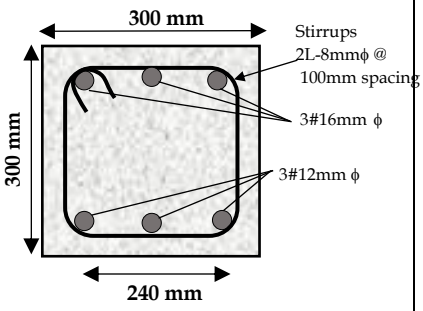	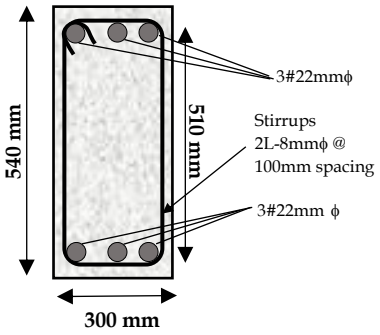
10S_60CR	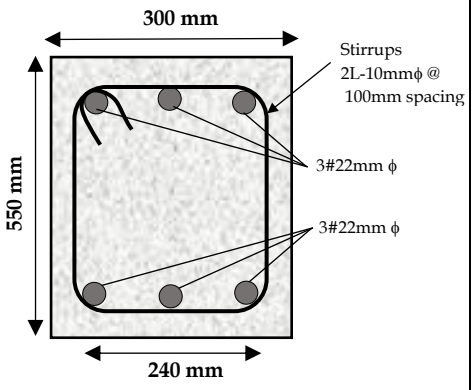	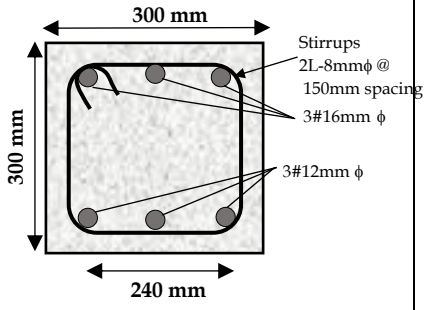	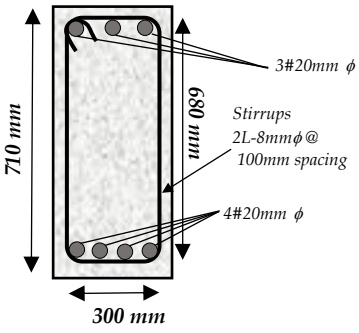
12S_40CR	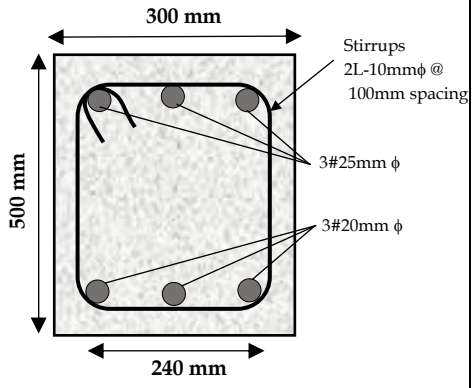	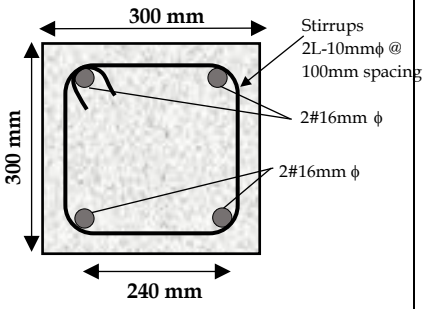	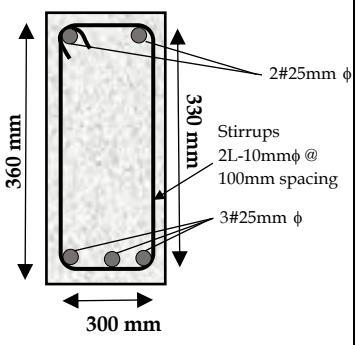

12S_50CR	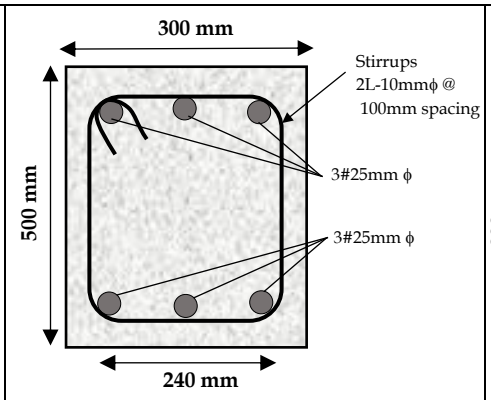	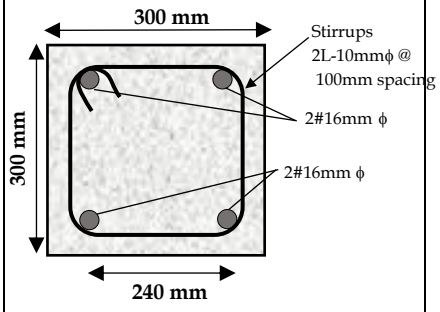	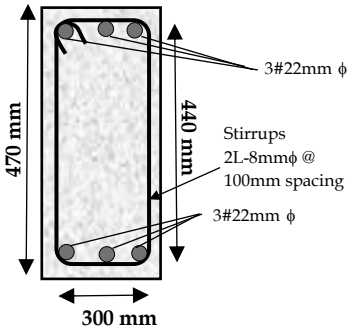
12S_60CR	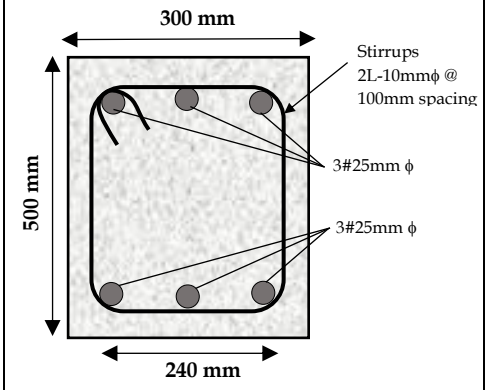	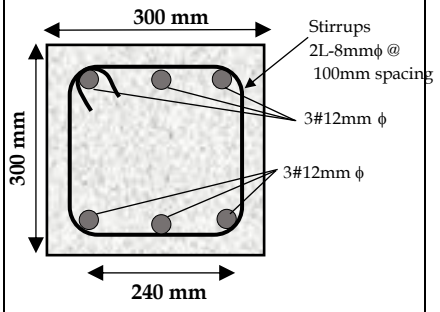	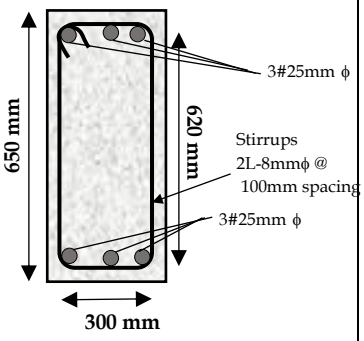
16S_40CR	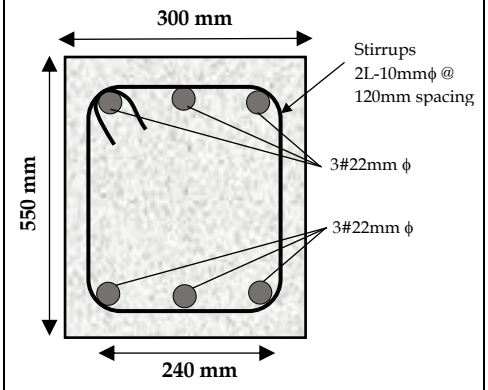	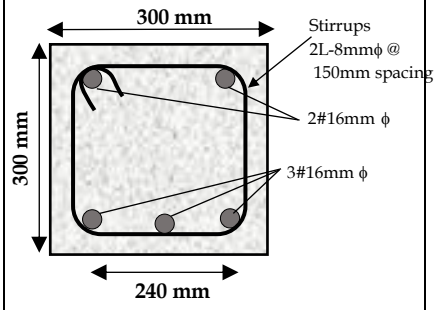	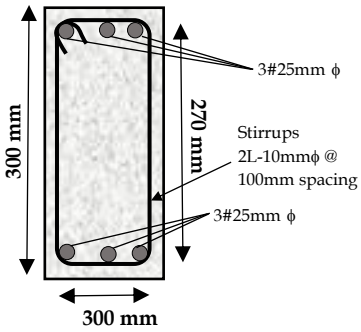
16S_50CR	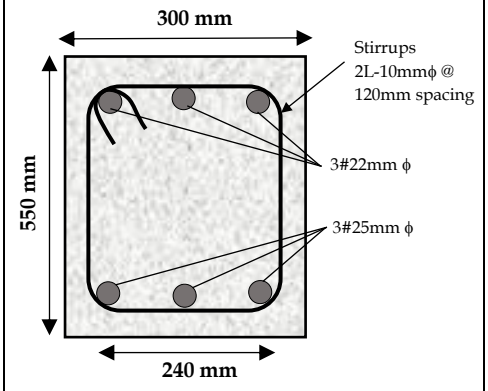	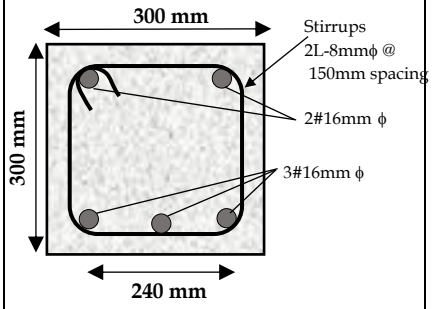	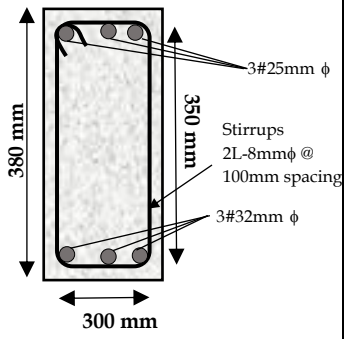

16S_60CR	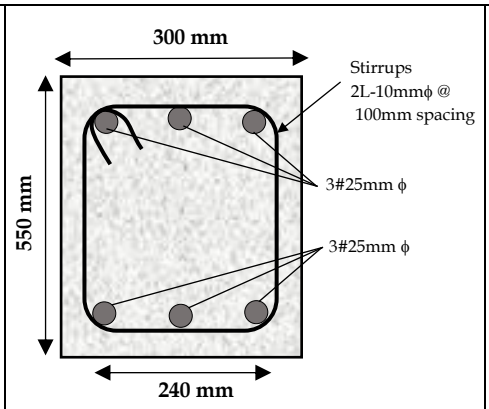	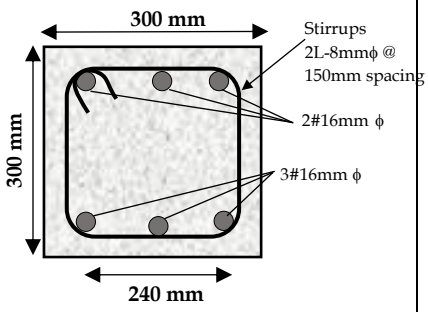	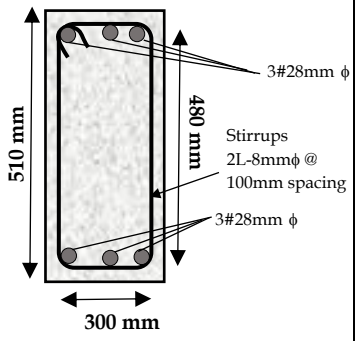
Note: *All cross-sectional profiles are illustrations and are not drawn to scale.*			

977

978 **A2. Detailing of Column**

10 Storey	12 Storey	16 Storey
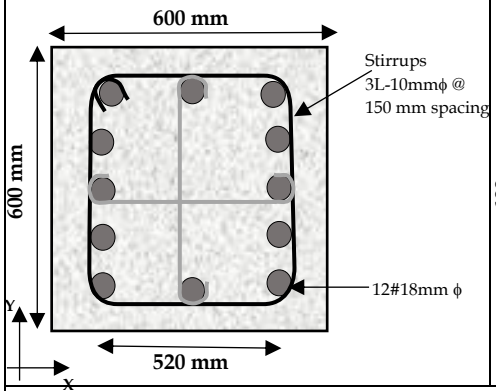	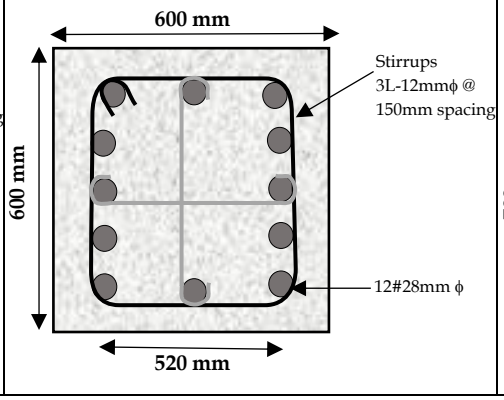	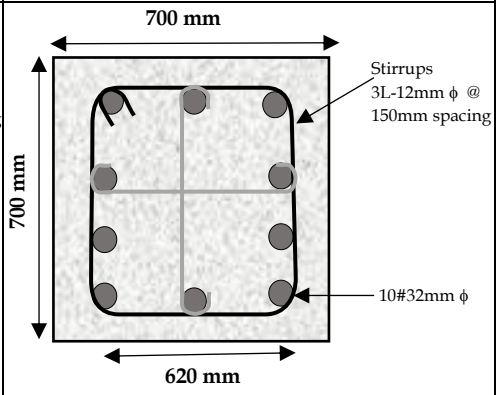
Note: *All cross-sectional profiles are illustrations and are not drawn to scale.*		

979

980 **A3. Detailing of Structural Wall**

981

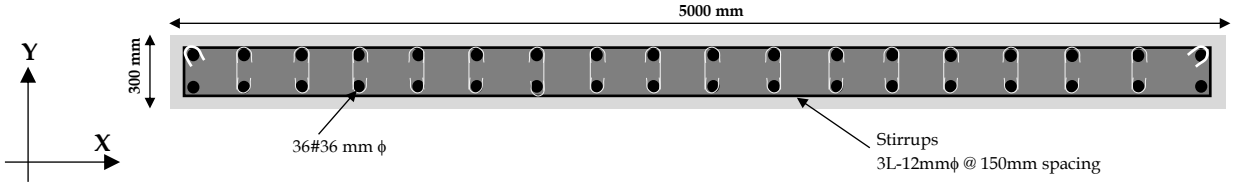

982

983

984

985

986

987

988

989

990

References

1. Niroomandi, A., Stevenson, C., Najafgholipour, M. A., Firoozbakhtian, M., & Sullivan, T. (2023). Seismic Behaviour of Slender Rectangular Reinforced Concrete Walls based on analytical methods. *Proceedings of the 2023 New Zealand Society for Earthquake Engineering Annual Technical Conference*.
2. IS 13920:2016 (2016) Indian standard code of practice on ductile design and detailing of reinforced concrete structures subjected to seismic forces. Bureau of Indian Standards, New Delhi, India.
3. Eljadei, A. A., & Harries, K. A. (2014). Design of coupled wall structures as evolving structural systems. *Engineering structures*, *73*, 100-113.
4. Binney JR, P. T. (1974). Diagonally reinforced concrete beams of shear walls. *ACI special publication*, *42*, 579-598.
5. Park, R., & Paulay, T. (1991). *Reinforced concrete structures*. John Wiley & Sons.
6. Harries, K. A. (2001). Ductility and deformability of coupling beams in reinforced concrete coupled walls. *Earthquake Spectra*, *17*(3), 457-478.
7. El-Tawil, S., & Kuenzli, C. M. (2002). Pushover of hybrid coupled walls. II: Analysis and behavior. *Journal of Structural Engineering*, *128*(10), 1282-1289.
8. El-Tawil, S., Harries, K. A., Fortney, P. J., Shahrooz, B. M., & Kurama, Y. (2010). Seismic design of hybrid coupled wall systems: state of the art. *Journal of structural engineering*, *136*(7), 755-769.
9. Lequesne, R. D. (2011). *Behavior and design of high-performance fiber-reinforced concrete coupling beams and coupled-wall systems* (Doctoral dissertation, university of Michigan).
10. Cheng, M. Y., Fikri, R., & Chen, C. C. (2015). Experimental study of reinforced concrete and hybrid coupled shear wall systems. *Engineering Structures*, *82*, 214-225.
11. Broberg, M., Shafaei, S., Kizilarslan, E., Seo, J., Varma, A. H., Bruneau, M., & Klemencic, R. (2022). Capacity design of coupled composite plate shear wall–concrete-filled system. *Journal of Structural Engineering*, *148*(4).
12. Zhou, Q., Su, M., Shi, Y., Guan, L., Lian, M., Jiang, L., ... & Zhang, L. (2021, December). Hysteretic behavior of the hybrid coupled partially encased composite wall system. In *Structures* (Vol. 34, pp. 4216-4236). Elsevier.
13. Hou, H., Wang, W., Alam, M. S., Wang, S., & Du, J. (2025). Experimental and Numerical Investigation on Seismic Performance and Yielding Sequence of Coupled-Double Skin Composite Walls. *Thin-Walled Structures*, 113646.
14. Liu, A., Wu, Y., Wang, B., & Chen, X. (2023). Seismic Design and Performance Evaluation of Coupled Steel Plate and Reinforced Concrete Composite Walls. *Buildings*, *13*(9), 2242.
15. Wu, X., Hao, J., Jiang, Y., Fu, H., Hou, X., & Ou, T. (2025). Coupling ratio and parametric analysis of coupled steel plate shear wall based on orthogonal test. *Thin-Walled Structures*, 113917.
16. Hernández-Montes, E., & Aschheim, M. (2017). An estimate of the yield displacement of coupled walls for seismic design. *International Journal of Concrete Structures and Materials*, *11*(2), 275-284.
17. Egyptian Code for Design and Construction of Reinforced Concrete Buildings (ECP-203), Research Center for Housing and Building, Giza, Egypt.
18. Eurocode 8: Design of structures for earthquake resistance-part 1: general rules, seismic actions and rules for buildings. Brussels: European Committee for Standardization.
19. Harries, K. A., Moulton, J. D. L., & Clemson, R. L. (2004). Parametric study of coupled wall behavior—implications for the design of coupling beams. *Journal of Structural Engineering*, *130*(3), 480-488.
20. IS 1893 (part 1): 2016—Indian standard criteria for earthquake resistant design of structures, part 1: general provisions and buildings (Sixth Revision). Bureau of Indian Standards, New Delhi.
21. Rossi, A., Del Vecchio, C., & Pampanin, S. (2022). Influence of earthquake damage and repair interventions on expected annual losses of reinforced concrete wall buildings. *Earthquake Spectra*, *38*(3), 2026-2060.
22. Cuevas, A., & Pampanin, S. (2017). Post Seismic Capacity of Damaged and Repaired Reinforced Concrete Plastic Hinges Extracted from a Real Building.
23. Gulkan, P. L., & Utkutuğ, D. (2003). Minimum design criteria for earthquake safety of school buildings. *Türkiye Mühendislik Haberleri*, *425*(3), 13-22.
24. Soydaş, O. (2009). *Evaluation of shear wall indexes for reinforced concrete buildings* (Master's thesis, Middle East Technical University).
25. Fox, M. J., Sullivan, T. J., & Beyer, K. (2014). Comparison of force-based and displacement-based design approaches for RC coupled walls in New Zealand. Bulletin of the New Zealand Society for Earthquake Engineering, 47(3), 190-205.
26. Jafari, A., Beheshti, M., Shahmansouri, A. A., &Bengar, H. A. (2024, March). Cyclic response and damage status of coupled and hybrid-coupled shear walls. In Structures (Vol. 61, p. 106010). Elsevier.
27. Rivard, G., Ambroise, S., & Paultre, P. (2022). Inelastic seismic shear amplification due to higher mode effects in reinforced concrete coupled walls. Earthquake Spectra, 38(2), 1357-1381.
28. Janevski, A., & Isaković, T. (2025). Seismic response of RC walls coupled by slabs without coupling beams. Engineering Structures, 329, 119861.

29. Khademi, M., Tehranizadeh, M., Shirkhani, A., Hajirasouliha, I., & Yang, T. Y. (2024, December). Effects of near-field pulse-like ground motions on the seismic resilience of RC shear wall buildings. In Structures (Vol. 70, p. 107585). Elsevier.
30. Castillo, J. G. S., Bruneau, M., &Elhami-Khorasani, N. (2022). Seismic resilience of building inventory towards resilient cities. Resilient Cities and Structures, 1(1), 1-12.
31. Joo, M. R., Badal, P. S., & Sinha, R. (2022, November). Recovery-based seismic resilience assessment of IS code-conforming RC buildings. In Symposium in Earthquake Engineering (pp. 95-110). Singapore: Springer Nature Singapore.
32. Computers & Structures Inc. [2020] ETABS [computer software], Berkeley, California.
33. Farahi, M., Freddi, F., & Latour, M. (2023). Seismic performance of self-centering hybrid coupled wall systems: Preliminary assessments. *Procedia Structural Integrity*, *44*, 1933-1939.
34. Fox, M., Sullivan, T., & Beyer, K. (2014). A case study in the capacity design of RC coupled walls. In *2nd European Conference on Earthquake Engineering and Seismology*.
35. Indian Standard IS: 456 – 2000, 'Plain and Reinforced Concrete – Code of Practice' (Fourth Revision), Tenth Reprint April 2007, Bureau of Indian Standards, Manak Bhavan, 9 Bahadur Shah Zafar Marg, New Delhi, India.
36. IS 875 (Part 2): 1987, Indian Standard Code of practice for Design loads (other than earthquake) for buildings and structures, Part 2 Imposed Loads (Second Revision).
37. Harries, K. A., Gong, B., & Shahrooz, B. M. (2000). Behavior and design of reinforced concrete, steel, and steel-concrete coupling beams. *Earthquake Spectra*, *16*(4), 775-799.
38. Fintel, M., & Ghosh, S. K. (1982). Case Study of Aseismic Design of a 16 Story Coupled Wall Structure Using Inelastic Dynamic Analysis. In *Journal Proceedings* (Vol. 79, No. 3, pp. 171-179).
39. Kurama, Y. C., Weldon, B. D., & Shen, Q. (2006). Experimental evaluation of posttensioned hybrid coupled wall subassemblages. *Journal of Structural Engineering*, *132*(7), 1017-1029.
40. Wallace, J. W. (2012). Behavior, design, and modeling of structural walls and coupling beams—Lessons from recent laboratory tests and earthquakes. *International Journal of Concrete Structures and Materials*, *6*, 3-18.
41. Paulay, T., & Priestley, M. N. (1992). *Seismic design of reinforced concrete and masonry buildings* (Vol. 768). New York: Wiley.
42. Haselton, C. B. (2006). *Assessing seismic collapse safety of modern reinforced concrete moment frame buildings* (Doctoral dissertation, Stanford University).
43. Ibarra, L. F., Medina, R. A., & Krawinkler, H. (2005). Hysteretic models that incorporate strength and stiffness deterioration. *Earthquake engineering & structural dynamics*, *34*(12), 1489-1511.
44. Orakcal, K., & Wallace, J. W. (2006). Flexural modeling of reinforced concrete walls-experimental verification. ACI Materials Journal, 103(2), 196.
45. Mander, J. B., Priestley, M. J., & Park, R. (1988). Theoretical stress-strain model for confined concrete. *Journal of structural engineering*, *114*(8), 1804-1826.
46. American Society of Civil Engineers (ASCE). Seismic Evaluation and Retrofit of Existing Buildings (ASCE 41-17). Reston, VA; 2017.
47. SP 16 (1980): Design Aids for Reinforced Concrete to IS 456: 1978
48. Vijayanarayanan, A. R., Goswami, R., & Murty, C. V. R. (2022). A method for seismic design of RC frame buildings using fundamental mode and plastic rotation capacity. *Bulletin of the New Zealand Society for Earthquake Engineering*, *55*(2), 112-128.
49. FEMA. (2005). 440, Improvement of nonlinear static seismic analysis procedures. *FEMA-440, Redwood City*, *7*(9), 11.
50. Arnold, C., FAIA, & RIBA. (2001). Architectural considerations. In *The seismic design handbook* (pp. 275-326). Boston, MA: Springer US.
51. Arnold, C., & Reitherman, R. (1982). Building configuration and seismic design. *John Wiley & Sons, New York.*
52. HAZUS, M. (2003). Multi-hazard loss estimation methodology. *Earthquake Model (HAZUS MH. MR4) Technical Manual. Department of Homeland Security, Emergency Preparedness and Response Directorate, FEMA*.
53. Benoy, S., Vijayanarayanan, A. R., & Saravanan, M. (2023). Paradigm shift to resilience based design for improved seismic behaviour–State-of-the-Art. *Materials Today: Proceedings*.
54. Cimellaro, G. P., Reinhorn, A. M., & Bruneau, M. (2010). Seismic resilience of a hospital system. *Structure and Infrastructure Engineering*, *6*(1-2), 127-144.
55. Castillo, J. G. S., Bruneau, M., & Elhami-Khorasani, N. (2022). Seismic resilience of building inventory towards resilient cities. *Resilient Cities and Structures*, *1*(1), 1-12.
56. Mahini SS, Setunge S, Hadigheh SA (2015) Performance vs resilience-based earthquake design for low and medium-rise retrofitted RC buildings. *In: Proceedings of the Tenth Pacific Conference on Earthquake Engineering Building an Earthquake-Resilient Pacific*, November 6-8, Sydney, Australia
57. Cimellaro, G. P., Reinhorn, A. M., & Bruneau, M. (2010). Framework for analytical quantification of disaster resilience. *Engineering structures*, *32*(11), 3639-3649.

58. Joseph, L., Madhavan, M. K., Jayanarayanan, K., & Pegoretti, A. (2023). Evaluation of hybrid fiber multiscale polymer composites for structural confinement under cyclic axial compressive loading. *Journal of Composites Science*, *7*(4), 152.
59. Benoy, S., Anusree, C. P., Saravanan, M., Zeneeb, A. M., & Vijayanarayanan, A. R. (2025, April). Analytical equations to estimate design biaxial response of high strength concrete structural walls. In *Structures* (Vol. 74, p. 108486). Elsevier.
60. Varma, D. A., Joseph, L., Madhavan, M. K., Jayanarayanan, K., & Pegoretti, A. (2024). Strength, durability and finite element analysis of hybrid jute/basalt fiber reinforced polymer confined concrete column under axial compression. *Results in Engineering*, *22*, 102281.
61. Hadigheh, S. A., Mahini, S. S., Setunge, S., & Mahin, S. A. (2016). A preliminary case study of resilience and performance of rehabilitated buildings subjected to earthquakes. *Earthq. Struct,* 11(6), 967-982.
62. Prasanth, S., & Ghosh, G. (2021, December). Effect of cracked section properties on the resilience based seismic performance evaluation of a building. In *Structures* (Vol. 34, pp. 1021-1033). Elsevier.